Accurate *ab initio* potential energy surface, dynamics, and thermochemistry of the $F+CH_4 \rightarrow HF+CH_3$ reaction

Gábor Czakó,[a] Benjamin C. Shepler, Bastiaan J. Braams, and Joel M. Bowman[b]
Cherry L. Emerson Center for Scientific Computation and Department of Chemistry, Emory University, Atlanta, Georgia 30322, USA

(Received 23 October 2008; accepted 18 December 2008; published online 24 February 2009)

An accurate full-dimensional global potential energy surface (PES) for the $F+CH_4 \rightarrow HF+CH_3$ reaction has been developed based on 19 384 UCCSD(T)/aug-cc-pVTZ quality *ab initio* energy points obtained by an efficient composite method employing explicit UCCSD(T)/aug-cc-pVDZ and UMP2/aug-cc-pV*XZ* [X=D,T] computations. The PES contains a first-order saddle point, $(CH_4\text{- -}F)_{SP}$, separating reactants from products, and also minima describing the van der Waals complexes, $(CH_4\text{- - -}F)_{vdW}$ and $(CH_3\text{- - -}HF)_{vdW}$, in the entrance and exit channels, respectively. The structures of these stationary points, as well as those of the reactants and products have been computed and the corresponding energies have been determined using basis set extrapolation techniques considering (a) electron correlation beyond the CCSD(T) level, (b) effects of the scalar relativity and the spin-orbit couplings, (c) diagonal Born–Oppenheimer corrections (DBOC), and (d) zero-point vibrational energies and thermal correction to the enthalpy at 298 K. The resulting saddle point barrier and ground state vibrationally adiabatic barrier heights (V_{SP} and V_{VAGS}), dissociation energy of $(CH_3\text{- - -}HF)_{vdW}$ (D_e and D_0), and the reaction enthalpy (ΔH_e°, ΔH_0°, and ΔH_{298}°) are (240 ± 40 and 245 ± 200 cm^{-1}), (1070 ± 10 and 460 ± 50 cm^{-1}), and (-10000 ± 50, -11200 ± 80, and -11000 ± 80 cm^{-1}), respectively. Variational vibrational calculations have been carried out for $(CH_3\text{- - -}HF)_{vdW}$ in full (12) dimensions. Quasiclassical trajectory calculations of the reaction using the new PES are reported. The computed HF vibrational and rotational distributions are in excellent agreement with experiment. © *2009 American Institute of Physics*.
[DOI: 10.1063/1.3068528]

I. INTRODUCTION

There have been many experimental and theoretical studies of the gas-phase reactions of a halogen atom and a hydride molecule, e.g., H_2, NH_3, CH_4, and their isotopologues.[1–13] Among the atom+diatom systems the $F+H_2 \rightarrow HF(v,J)+H$ reaction has received a lot of attention (see the review Ref. 1). Since an atom+diatom system has "only" three internal degrees of freedom, the dynamics of the above-mentioned reaction have been studied by sophisticated theoretical methods, i.e., using a highly accurate *ab initio*-based potential energy surface (PES) and quantum dynamics of the nuclear motion. In the case of the collision between an atom and a polyatomic molecule, the number of internal degrees of freedom ($3N-6$) increases with the number of atoms (N). Therefore, *ab initio*, quantum simulation of the reaction dynamics is increasingly challenging, mainly due to exponential scaling of the total effort with respect to the number of electrons and the number of nuclei. As a result, quasiclassical trajectory (QCT) calculations are frequently used in order to describe the nuclear dynamics of these reactions. The QCT method propagates the nuclei classically while the required forces, i.e., potential gradients, are computed quantum mechanically by solving the related electronic Schrödinger equation. In a typical QCT calculation a large number of electronic energy gradients, e.g., around 10^7-10^8 are required. There are different strategies to obtain these electronic energies and gradients for the QCT calculations. One increasingly popular approach is "direct dynamics," where these quantities are obtained "on the fly" employing a standard electronic structure program package. This approach has a serious limitation, since the calculation of around 10^7-10^8 energy gradients using high-level *ab initio* methods is currently not feasible. Another approach employs an analytical representation of the PES, which allows inexpensive calculation of the required gradients by analytical or numerical differentiation of the PES. A third approach uses a relatively efficient semiempirical electronic structure method with parameters optimized for a specific reaction. All of these approaches have been applied to the title reaction (and other polyatomic reactions) and some of these will be reviewed below and in Sec. III, where we describe the approach developed in our group to represent PESs in high dimensionality and give the details of the implementation to the title reaction.

The $F+CH_4 \rightarrow HF(v,J)+CH_3$ reaction plays an important role in the atmosphere and stratosphere. A schematic of the stationary points of this reaction is shown in Fig. 1. The reaction has a so-called early saddle point, $(CH_4\text{- -}F)_{SP}$, whose structure is similar to that of the reactants. Furthermore, there is a shallow van der Waals (vdW) valley,

[a]Author to whom correspondence should be addressed. Electronic mail: czako@chem.elte.hu.
[b]Electronic mail: jmbowma@emory.edu.

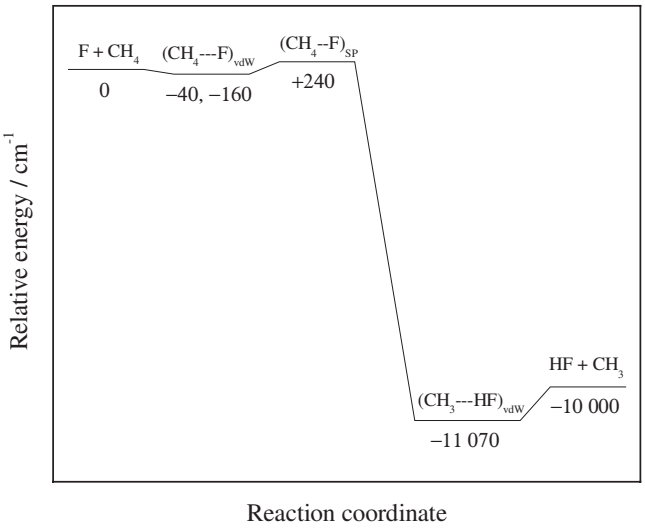

FIG. 1. Schematic potential energy surface of the $F+CH_4 \rightarrow HF+CH_3$ reaction. For computational details for the given accurate vibrationless relative energies, see Tables VIII and XIV. Relative energies, -40 and -160 cm^{-1}, correspond to a second-order saddle point and a minimum in the vdW well, respectively.

$(CH_4\text{- - -}F)_{vdW}$, in the entrance channel, but very little has been known about the energetics and structure(s) of the complex(es) in this well. The reaction is very exothermic and there is a relatively deep vdW minimum, $(CH_3\text{- - -}HF)_{vdW}$, in the product valley, whose vibrationless energy is below the product asymptote by about 1100 cm^{-1}. Hereafter we denote these stationary points as SP, vdWR, vdWP, respectively.

Previous published *ab initio* structures of these stationary points are summarized in Table I. Most of the studies predicted a collinear (C_{3v}) saddle point structure.[6,7,14] Others,[8,9] using higher levels of theory, gave a bent (C_s) SP structure, which is supported by experiment.[11] The previous thermochemical data including the barrier height, dissociation energy of vdWP, and the reaction enthalpy are given in Table II. In 2005 Roberto-Neto and co-workers[9] reported that their best values for the barrier height and the enthalpy of the reaction were computed at the CCSD(T)/cc-pVTZ and CCSD(T)/aug-cc-pVQZ levels of theory, respectively. The authors stated that "further improvements in these results with the extension of the basis set is very costly."[9] In the present paper we report the best technically feasible *ab initio* values for the structural parameters and thermochemical properties of the title reaction employing the so-called focal-point analysis (FPA) approach.[15–17] This FPA study supersedes previous work by considering (a) basis set extrapolation techniques to approach the complete basis set (CBS) limit; (b) electron correlation methods beyond the "gold standard" CCSD(T) level; (c) effects of the scalar relativity and the spin-orbit (SO) couplings; (d) diagonal Born–Oppenheimer corrections (DBOC); (e) variationally computed fully anharmonic (harmonic for the SP) zero-point vibrational energy (ZPVE) corrections. Furthermore, unlike most of the previous work, our FPA study employs all-electron (AE) methods for treating the electron correlation.

A concise review of previous PESs and QCT studies of the title reaction is presented in Table III and its footnotes. In 2005 Troya[8] published a QCT study using a specific-reaction-parameter parameter-model 3 (SRP-PM3) semi-empirical Hamiltonian, which provided the best agreement with the measured HF vibrational and rotational distributions[11] to date. It is important to note that the best *ab initio* full-dimensional PES in the literature was computed at frozen-core UMP2/aug-cc-pVDZ level.[7] In order to decrease the seriously overestimated barrier height the scaling-all-correlation[18] (SAC) method was employed. This PES was constructed using a so-called Shepard-interpolation method based on 1100 data points (energies and first and second derivatives). However, the computed HF rovibrational distribution was not in agreement with experiment. The authors concluded "to further improve the agreement with experimental results and to explain in detail the interesting findings derived from the most recent experiments, higher level *ab initio* calculations for the PES and/or the concurrence of quantum mechanical scattering calculations may be required."[7]

In this paper we present a full-dimensional *ab initio*-based PES by fitting 19384 energies obtained using a composite method that, as we show, yields energies of near frozen-core UCCSD(T)/aug-cc-pVTZ quality. QCT calculations have been carried out using this new PES, and the

TABLE I. Literature data for the *ab initio* structures of the saddle point $(CH_4\text{- -}F)_{SP}$ and the product vdW complex $(CH_3\text{- - -}HF)_{vdW}$.

Methods	Symmetry	$r(CH_b)$[a]	$r(H_bF)$[a]	$\alpha(CH_bF)$[a]	Authors and references
		Saddle point			
QCISD/6-311+G(2*df*,2*pd*)	C_{3v}	1.114	1.552	180.0	Troya *et al.* (2004) (Ref. 6)
CCSD(T)/cc-pVTZ	C_s	1.177	1.537	177.2	Roberto-Neto *et al.* (2005) (Ref. 9)
QCISD/cc-pVTZ	C_{3v}	1.124	1.483	180.0	Castillo *et al.* (2005) (Ref. 7)
UCCSD(T)/aug-cc-pVDZ	C_s	1.124	1.643	153.4	Troya (2005) (Ref. 8)
UMP2/6-311+G(2*df*,2*dp*)[b]	C_{3v}	1.125	1.435	180.0	Wang *et al.* (2006) (Ref. 14)
		Product vdW complex			
UMP2/6-311+G(2*df*,2*pd*)	C_{3v}	2.138	0.924	180.0	Troya *et al.* (2004) (Ref. 6)
QCISD/aug-cc-pVDZ	C_{3v}	2.286	0.928	180.0	Castillo *et al.* (2005) (Ref. 7)

[a]All the bond lengths (r) are in angstroms, and the bond angles (α) are in degrees (see Fig. 2 for the notations).
[b]In the footnote of Table I of Ref. 14, the QCISD(T)/6-311++G(2*df*,2*dp*) level is given, but we are confident that the UMP2/6-311+G(2*df*,2*dp*) level was employed as stated in the text of the same paper.

TABLE II. Literature data for the *ab initio* thermochemistry of the F+CH$_4$→HF+CH$_3$ reaction.

Barrier height[a]			
Methods	V_{SP}	V_{VAGS}	Authors and references
QCISD(T)//QCISD/6-311+G(2*df*,2*pd*)	161	−227	Troya *et al.* (2004) (Ref. 6)
CCSD(T)/cc-pVTZ	630	175	Roberto-Neto *et al.* (2005) (Ref. 9)
QCISD(T)/aug-cc-pVTZ//QCISD/cc-pVTZ	−220	−752	Castillo *et al.* (2005) (Ref. 7)
CCSD(T)/aug-cc-pVTZ//CCSD(T)/aug-cc-pVDZ	140	−122	Troya (2005) (Ref. 8)

Dissociation energy of $(CH_3\text{- - -HF})_{vdW}$[a]			
Methods	D_e	D_0	Authors and references
UMP2/6-311+G(2*df*,2*pd*)	1098	479	Troya *et al.* (2004) (Ref. 6)
QCISD/aug-cc-pVDZ	797	262	Castillo *et al.* (2005) (Ref. 7)

Enthalpy of the reaction[a]			
Methods	ΔH_e°	ΔH_0°	Authors and references
QCISD(T)//QCISD/6-311+G(2*df*,2*pd*)	−9910	−11130	Troya *et al.* (2004) (Ref. 6)
CCSD(T)/aug-cc-pVQZ(cc-pVQZ)[b]	−10110	−11020[b]	Roberto-Neto *et al.* (2005) (Ref. 9)
QCISD(T)/aug-cc-pVTZ//QCISD/cc-pVTZ	−9860	−11070	Castillo *et al.* (2005) (Ref. 7)
CCSD(T)/aug-cc-pVTZ//CCSD(T)/aug-cc-pVDZ	−9770	−10970	Troya (2005) (Ref. 8)

[a]All the data are given in cm^{-1}. Note that they were originally reported in kcal/mol.
[b]The ΔH_0° was computed at CCSD(T)/cc-pVQZ level, and the value of ΔH_{298}° was also given as −11 510 cm^{-1} at the same level of theory.

computed HF vibrational and rotational distributions are compared to experiment. In addition 12-dimensional variational vibrational calculations are performed for $(CH_3\text{- - -HF})_{vdW}$, and these could provide guidance for any future experimental investigation of the spectroscopy of this complex. Since the present paper focuses on the description of the global PES and the high-level *ab initio* characterization of the stationary points relevant for the title reaction, we do plan a subsequent paper with a more extensive study of the dynamics, which are only briefly described in this paper.

II. COMPUTATIONAL METHODS

The electronic structure calculations employed the augmented correlation-consistent polarized (Core)/Valence *X* Zeta, aug-cc-p(C)V*XZ* [*X*=2(D), 3(T), 4(Q), 5, and 6], basis sets.[19–21] For the single-reference correlation methods, the reference electronic wave functions were determined by the single-configuration restricted as well as unrestricted open-shell Hartree–Fock (ROHF and UHF) methods.[22] The restricted and unrestricted open-shell second-order Møller–Plesset perturbation theory[23] (RMP2 and UMP2) and the coupled-cluster (CC) (Ref. 24) methods including all single and double (CCSD), triple (CCSDT), and quadruple (CCSDTQ) excitations as well as the CCSD(T) (Refs. 25 and 26) and CCSDT(Q) (Ref. 27) methods including perturbative triple (T) and quadruple (Q) terms were employed to account for electron correlation. Note that for closed-shell systems, i.e., CH$_4$ and HF, restricted Hartree–Fock (RHF) reference function with fully restricted formalism of the correlation methods was employed.[25] For open-shell systems the CC method can also be either restricted or unrestricted. Restricted CC methods are based on ROHF reference electronic wave functions, therefore the restricted CC methods are denoted as RCC, e.g., RCCSD and RCCSD(T). However, unrestricted CC (UCC) methods have been developed using both ROHF and UHF reference functions. Up to the UCCSD(T) level we employed both the ROHF-UCC and UHF-UCC methods. The post-UCCSD(T) computations were performed based on UHF orbitals. In the present application the RCC and UCC results can differ from each other by about 30–150 cm^{-1}, whereas the difference between the ROHF-UCC and UHF-UCC energies is as small as 1–5 cm^{-1}. Note that this difference decreases when high-order excitations are included in the UCC series. Therefore, after defining the employed UCC methods precisely in this section, the UCC abbreviation will be used; regardless UCC is based on either ROHF or UHF references, unless we want to emphasize the reference function. Finally, we note that in this study FC denotes the use of the usual frozen-core approach, i.e., the 1*s*-like core orbitals corresponding to C and F atoms are kept frozen, for the electron correlation calculations, while AE means computations when all the electrons are correlated.

Geometry optimizations at RMP2 and UMP2 as well as RCCSD(T) and ROHF-UCCSD(T) levels and harmonic frequency computations with the ROHF-UCCSD(T) method were performed by the program package MOLPRO.[28] All the single-point energies for the FPA approach up to the AE-ROHF-UCCSD(T) level were also computed by MOLPRO. The MRCC program[29,30] [interfaced to ACESII (Ref. 31)] was employed for the AE UHF-UCCSDT, UHF-UCCSDT(Q), and UHF-UCCSDTQ computations. The diagonal DBOC (Ref. 32) were determined by the program packages PSI (Ref. 33) and ACESII. The scalar relativistic effects were taken into account by using the Douglas–Kroll[34] relativistic one-electron integrals as implemented in MOLPRO. All the multireference configuration interaction (MRCI+Q) computations using the Davidson correction to estimate the effect of the higher-order excitations (+Q) as well as the spin-orbit coupling calculations with the Breit–Pauli operator in the inter-

TABLE III. Potential energy surfaces and quasiclassical trajectory studies in the literature for the $F+CH_4 \rightarrow HF+CH_3$ reaction.

Keywords	Authors and references	Comments
Semiempirical, three dimension, three-parameter LEPS	Gauss, Jr. (1976) (Ref. 2)	[a]
Semiempirical, two PESs; both fitted to expt., one also to theory	Corchado *et al.* (1996) (Ref. 3)	[b]
Semiempirical, optimized for expt. thermal rate constant	Kornweitz *et al.* (1998) (Ref. 4)	[c]
Ab initio at PUMP4//UMP2/6-311+G(2*df*,2*pd*), 3 dimension	Troya *et al.* (2004) (Ref. 6)	[d]
Semiempirical, two PESs, one of them includes SO correction for F	Rángel *et al.* (2005) (Ref. 5)	[e]
Ab initio full dim. at UMP2(-SAC)/aug-cc-pVDZ, interpolated	Castillo *et al.* (2005) (Ref. 7)	[f]
Semiempirical reparametrized Hamiltonian (SRP-PM3)	Troya (2005) (Ref. 8)	[g]
Semiempirical, reconstructed PES, improved rovibrational distribution	Espinosa-García *et al.* (2007) (Ref. 10)	[h]

[a]CH_4F was treated as a three-body system (F, H, CH_3), and a three-parameter LEPS (London, Eyring, Polanyi, Sato) potential was developed. The three Sato parameters were determined from experimental data.

[b]Two semiempirical surfaces, the so-called MJ1 and PM3-SRP, were developed. MJ1 is a slightly modified version of the analytic function (J1) for the $H+CH_4 \rightarrow H_2+CH_3$ reaction. MJ1 was calibrated with respect to the experimental reactant and products properties as well as to the *ab initio* saddle point data. PM3-SRP was based on the PM3 semiempirical molecular orbital theory using parameters specifically calculated for the title reaction (SRP method). PM3-SRP was fitted to experiment, but not to the *ab initio* data.

[c]The PES was obtained from the potential of the $H+CH_4$ reaction by modifying a few parameters. The new PES was optimized with respect to the experimental thermal rate constant. The computed HF vibrational distribution was in good agreement with experiment, although the $v=3$ state was overpopulated.

[d]Analytic potential, using a triatomic (F, H, CH_3) model, was computed at the AE PUMP4//UMP2/6-311+G(2*df*,2*pd*) level. The three-body term was fitted to 103 *ab initio* points. The final rms error was 1.70 kcal/mol. Detailed QCT study was presented for the title reaction, where the vibrational and rotational distributions of HF were obtained.

[e]Two semiempirical surfaces (PES-SO and PES-NOSO) were developed and calibrated with respect to the saddle point properties and the experimental thermal rate constants. PES-SO corresponds to the spin-orbit ground state of the F atom ($^2P_{3/2}$), while PES-NOSO takes the averaged energy of the two spin-orbit states. PES-NOSO surface reproduced better experimental rate constants. Note that these surfaces neglect the vdW minimum in the product valley. Troya computed the HF vibrational and rotational distributions using the PES-NOSO surface and the agreement with experiment was not good. Especially the rotational states corresponding to high J values were seriously overpopulated. The saga continues at footnote h.

[f]The first full-dimensional *ab initio* interpolated PES was reported. The total of 1100 data points (energies and first and second derivatives) were computed at frozen-core UMP2/aug-cc-pVDZ level. Since MP2 seriously overestimates the barrier height, the SAC method was also employed in order to make the barrier lower. The QCT calculations predicted that the accessible HF vibrational levels were almost equally populated. This result does not agree with experiment.

[g]The parameter-model 3 (PM3) semiempirical Hamiltonian was reparametrized using high-level *ab initio* data. The QCT calculations with the SRP PM3 semiempirical Hamiltonian reproduced quantitatively the measured HF vibrational distribution.

[h]The former PES-NOSO (see footnote e.) surface was reconstructed in order to improve the agreement with the experimental HF vibrational and rotational distributions. The former PES showed much less HF vibrational excitation and produced much hotter rotational distribution than it was seen in experiment. The new PES improved the vibrational and rotational distributions, but the HF rotational population for the $v=2$ state was still too hot. Note that the new PES does have the vdW complex in the product valley, but no complex was found in the entry channel.

acting states approach[35] were also performed by MOLPRO. The energy points for the PES at the FC-UHF-UCCSD(T)/aug-cc-pVDZ level were computed by the GAUSSIAN program package,[36] while all the other energies were obtained by MOLPRO (see below for more details about the calculations specifically for the PES).

For the polyatomic species, the variational vibrational calculations were performed by the program package MULTIMODE (MM) (Refs. 37 and 38) using the vibrational configuration interaction (VCI) method. MM employs the finite basis representation of the Watson Hamiltonian[39] using the so-called n-mode representation (nMR) (Refs. 40 and 41) for the potential and the inverse of the effective moment of inertia. In the VCI basis all i-mode excitations, where $i=1-5$, are simultaneously allowed to a maximum of N_i quanta in each mode. Furthermore, an upper limit of the sum of the quanta is set to M_i for the corresponding i-mode basis functions. In this paper let us denote a basis set as $[N_{1M_1},\ldots,N_{i_{\max}M_{i_{\max}}}]$, where the maximum number of the simultaneously excited modes is $i_{\max}$. In this study most of the VCI calculations employed 4MR; since it was demonstrated in several previous studies[42,43] the 4MR gives vibrational energy levels within about 1 cm^{-1} corresponding to the given PES. For more details concerning to the MM calculations see Ref. 43.

The QCT calculations were performed using our own FORTRAN program, which has been employed in several simi-

TABLE IV. Test of the composite method employed for the CH_4F system at different regions of the global PES.

r(CH) [a]	r(CH_b) [a]	r(H_bF) [a]	α(HCH$_b$) [a]	α(CH_bF) [a]	$\Delta E_{UMP2/aVDZ}$ [b]	$\Delta E_{UMP2/aVTZ}$ [b]	$\Delta E_{UCCSD(T)/aVDZ}$ [b]	ΔE_{PES} [b]	$E_{UCCSD(T)/aVTZ}$ [b]
1.081	2.137	0.929	93.4	180.0	0	0	0	0	0
1.100	4.000	0.900	90.0	180.0	−187	+61	−258	−9	1 260
1.100	3.500	1.000	100.0	180.0	−371	+1	−395	−23	2 542
1.100	1.500	1.000	90.0	180.0	−137	+100	−226	+11	3 171
1.100	2.000	0.900	110.0	150.0	−33	+72	−115	−10	3 198
1.100	2.500	1.100	100.0	90.0	−438	+96	−563	−29	6 928
1.200	3.000	1.000	90.0	120.0	−714	+537	−1312	−60	6 998
1.000	1.400	1.000	100.0	160.0	+985	−167	+1222	+70	7 664
1.100	1.100	4.000	109.5	180.0	+1197	+1803	−620	−14	10 956
1.100	3.000	1.200	95.0	140.0	−791	+42	−886	−53	10 974
1.100	1.100	1.500	100.0	150.0	+2545	+3108	−567	−4	12 287
1.100	1.300	1.800	100.0	120.0	+1917	+2906	−1019	−31	15 193
1.200	1.100	1.600	105.0	180.0	+1697	+3032	−1411	−76	15 547
1.200	1.200	3.000	109.5	180.0	+676	+2277	−1683	−82	16 299
1.000	1.200	1.800	115.0	180.0	+2159	+1678	+520	+39	19 189

[a]All the bond lengths (r) are in angstroms, and the bond angles (α) are in degrees. For the sake of clarity, $r(CH)=r(CH_1)=r(CH_2)$, $\alpha(HCH_b)=\alpha(H_1CH_b)=\alpha(H_2CH_b)$, and $\tau(H_2CH_bF)=120°$ (see Fig. 2 for the notations).
[b]$\Delta E_{UMP2/aVDZ}$, $\Delta E_{UMP2/aVTZ}$, $\Delta E_{UCCSD(T)/aVDZ}$, and ΔE_{PES} are the deviations (in cm^{-1}) from the corresponding $E_{UCCSD(T)/aVTZ}$ relative energy, where $E_{PES}=E_{UCCSD(T)/aVDZ}+E_{UMP2/aVTZ}-E_{UMP2/aVDZ}$ (for more details, see Sec. III). All the energies relative to the same reference configuration, which corresponds to the global minimum of the PES, i.e., vdW complex in the exit channel.

lar applications, e.g., see Ref. 44. The gradients required for propagating the trajectories in time were obtained by numerical differentiation of the PES. Further details of the QCT method and initial conditions for the present reaction are given in Sec. VII.

III. GLOBAL *AB INITIO* POTENTIAL ENERGY SURFACE

The computation of a full-dimensional global PES for the F+$CH_4 \rightarrow$HF+CH_3 reaction is challenging, not just because of the large number (12) of internal degrees of freedom, but due to the fact that F+CH_4 is an open-shell (doublet) system. Preliminary test calculations at certain regions of the PES, especially at large F- - -CH_4 separations, showed that there were convergence problems with the ROHF method, while UHF did converge properly. Therefore, UHF wave functions should be used as reference for the correlation methods. However, MOLPRO, the seemingly most efficient program package for single-point CCSD(T) calculations, cannot be employed due to the fact that CC methods based on a UHF reference are not implemented in that code. This practical problem motivated us to consider an alternate and, in fact, quite efficient composite approach, where the *ab initio* energies for the PES (E_{PES}) are obtained from the expression

$$E_{PES} = E_{UCCSD(T)/aVDZ} + E_{UMP2/aVTZ} - E_{UMP2/aVDZ}. \quad (1)$$

In Eq. (1) the energies, $E_{UCCSD(T)/aVDZ}$, $E_{UMP2/aVTZ}$, and $E_{UMP2/aVDZ}$, are computed at the frozen-core UHF-UCCSD(T)/aug-cc-pVDZ, UMP2/aug-cc-pVTZ, and UMP2/aug-cc-pVDZ levels of theory, respectively.

This composite approach was tested by performing the UHF-UCCSD(T)/aug-cc-pVTZ calculations at different regions of the PES, relevant for the dynamics of the title reaction. These test results are summarized in Table IV. All the considered energies are relative to the same reference configuration corresponding to the global minimum of the PES, i.e., vdW complex in the exit channel. Comparing to the UCCSD(T)/aug-cc-pVTZ results the rms error of the UMP2/aug-cc-pVDZ, UMP2/aug-cc-pVTZ, and UCCSD(T)/aug-cc-pVDZ relative energies are 1256, 1667, and 904 cm^{-1}, respectively, whereas the rms error of the composite approach is only 45 cm^{-1}. These results clearly show the excellent performance of this composite method. Furthermore, one can see from Table IV that UMP2 works even better than the UCCSD(T)/aug-cc-pVDZ level in the case of the "product-type" configurations, however, suffers from large errors at the "reactant-type" configurations; thus UMP2 cannot be employed to compute an accurate *global* PES. It is also interesting to note that the rms error increases with the size of the basis set at the UMP2 level. It shows that treatment of the electron correlation beyond the UMP2 level is important in order to achieve the accuracy sought in the present study. Furthermore, the relatively large rms error of the UCCSD(T)/aug-cc-pVDZ level indicates that the aug-cc-pVDZ basis is not complete enough to provide accurate results. Nevertheless, it is comforting to find that the composite approach performs almost as well as the computationally much more expensive UCCSD(T)/aug-cc-pVTZ level.

The total number of *ab initio* energies used in the fit is 19 384. Equation (1) has been employed to compute 12 384 data points in the complex region. Furthermore, 7000 configurations have been built up from fragment data: 2000 for CH_4+F, 2000 for CH_3+HF, 2000 for CH_2F+H_2, and 1000 for CH_3F+H. The energies for the doublets (CH_3, CH_2F, and F) have been obtained at the FC-UCCSD(T)/aug-cc-pVTZ level. *Ab initio* calculations for the closed-shell molecules, (HF, CH_4, and CH_3F) and H_2 have been performed at the FC-CCSD(T)/aug-cc-pVTZ and CISD/aug-cc-pVTZ levels, respectively. For the H atom the exact BO nonrelativistic energy, −0.5 E_h, has been used. Note that our global PES involves the CH_2F+H_2 and CH_3F+H channels beside the

TABLE V. Properties of the global PES of the $F+CH_4 \rightarrow HF+CH_3$ reaction.

$F+CH_4$				$(CH_4\text{- -F})_{SP}$				$(CH_3\text{- - -HF})_{vdW}$				$HF+CH_3$			
	PES[a]	aVTZ[b]	Acc.[c]		PES[a]	aVTZ[b]	Acc.[c]		PES[a]	aVTZ[b]	Acc.[c]		PES[a]	aVTZ[b]	Acc.[c]
Structures[d]															
r(CH)	1.091	1.090	1.087	$r(CH_1)$	1.091	1.090	1.088	r(CH)	1.083	1.081	1.078	r(CH)	1.081	1.080	1.077
				$r(CH_2)$	1.089	1.088	1.087								
				$r(CH_b)$	1.105	1.112	1.111	$r(CH_b)$	2.208	2.137	2.142				
				$r(H_bF)$	1.656	1.628	1.621	$r(H_bF)$	0.927	0.929	0.925	r(HF)	0.922	0.921	0.917
				$\alpha(H_1CH_b)$	106.5	107.3	107.2	$\alpha(HCH_b)$	93.9	93.4	93.1				
				$\alpha(H_2CH_b)$	108.6	108.3	108.3								
				$\alpha(CH_bF)$	144.4	152.5	152.3								
Relative energies (cm^{-1})															
	0	0	0		167	139	186		−11048	−10945	−11182		−9784	−9771	−10077

[a]Results corresponding to the global fitted PES.
[b]Results obtained by *ab initio* calculations at the frozen-core UCCSD(T)/aug-cc-pVTZ level of theory.
[c]Accurate results obtained for $(CH_4\text{- -F})_{SP}$ at the AE UCCSD(T)/aug-cc-pCVTZ and for all the other species at the AE UCCSD(T)/aug-cc-pCVQZ level of theory.
[d]All the bond lengths (r) are in angstroms and the bond angles (α) are in degrees. See Fig. 2 for the notations.

most relevant CH_3+HF product channel, but the detailed study of those higher-energy asymptotes is out of the scope of the present paper.

The PES is represented by a polynomial expansion in Morse-like variables of the internuclear distances, $y_{ij}=\exp(-r_{ij}/a)$ where $a=2.0$ bohr and using a compact polynomial basis that is explicitly invariant under permutations of like atoms. We included all terms up to total degree 6, and the total number of free coefficients is 3262. These were determined by a weighted linear least-squares fit, in which a configuration at energy E relative to the global minimum has weight $E_0/(E+E_0)$ where $E_0=0.05$ E_h. The rms fitting error is 125 cm^{-1} over the subset of configurations that have energy at most 11 000 cm^{-1} above the global minimum, increasing to 222 cm^{-1} for configurations having energy in the range of 11 000–22 000 cm^{-1}, and 536 cm^{-1} for the subset in the range of 22 000–55 000 cm^{-1}. The numbers of configurations in those three ranges are 1415, 6721, and 9502, respectively.

Properties of the global PES are given in Table V including the structures corresponding to the reactants ($F+CH_4$), the products ($HF+CH_3$), the saddle point $(CH_4\text{- -F})_{SP}$, and the vdW complex $(CH_3\text{- - -HF})_{vdW}$ as well as the relative energies with respect to the entrance channel. Relevant *ab initio* geometries are also shown computed at the FC-UCCSD(T)/aug-cc-pVTZ level of theory as this is the target quality of the energy points used for the fitting procedure. For comparison, results are also presented computed at high level of theory (see Sec. IV). The relative energies corresponding to the PES agree with the FC-UCCSD(T)/aug-cc-pVTZ results to within 28, 103, and 13 cm^{-1}, respectively for $(CH_4\text{- -F})_{SP}$, $(CH_3\text{- - -HF})_{vdW}$, and $HF+CH_3$. This demonstrates both the precision of the fit and the accuracy of the composite method employed in this study.

As discussed in more detail in Sec. IV the high levels of electronic structure theory give a noncollinear $C-H_b-F$ SP structure. To the best of our knowledge the present PES is the first in literature whose first-order saddle point corresponds to a bent structure. In the case of the reactant and product channels, the T_d and D_{3h} point-group symmetries of CH_4 and CH_3, respectively, have been obtained within the expected numerical precision and the CH bond lengths corresponding to the PES are in good agreement with the FC-UCCSD(T)/aug-cc-pVTZ *ab initio* values.

IV. STRUCTURES

A. Saddle point $(CH_4\text{- -F})_{SP}$

As it was mentioned earlier, the title reaction has a nonlinear $C-H_b-F$ SP structure of C_s point-group symmetry, as shown in Fig. 2. The SP structure was determined at different levels of theory and the results are summarized in Table VI. The best estimates for the equilibrium structural parameters have been obtained at the AE-UCCSD(T)/aug-cc-pCVTZ level of theory. The bond lengths $r(C-H_1)$, $r(C-H_2)$, $r(C-H_b)$, and $r(H_b-F)$, see Fig. 2, are 1.088, 1.087, 1.111, and 1.621 Å, respectively. The bond angles $\alpha(H_1-C-H_b)$, $\alpha(H_2-C-H_b)$, and $\alpha(C-H_b-F)$ are 107.2°, 108.3°, and 152.3°, respectively, while the torsion angle $\tau(H_2-C-H_b-F)$ is 119.8°. For comparison the CH distance in the free CH_4 is 1.088 Å at the same level of theory. As the results show the two CH distances, CH_1 and CH_2, differ by 0.001 Å due to the lost C_{3v} symmetry. The CH_b bond length is stretched by 0.023 Å with respect to the bond length in the free CH_4 and the split bond angles, $\alpha(H_1-C-H_b)$ and $\alpha(H_2-C-H_b)$, are decreased by 2.3° and 1.2°, respectively, relative to the tetrahedral angle (109.5°) of CH_4. Due to the fact that these perturbations in the bond lengths and angles of the CH_4 unit at the saddle point are relatively small, this "qualifies" this as an "early saddle point." As expected both the H_b-F equilibrium distance and the $C-H_b-F$ angle are very sensitive to the level of theory. However, perhaps unexpectedly, even the same methods with either restricted or unrestricted formalism, FC-RCCSD(T) and FC-UCCSD(T), give $r(H_b-F)$ values of 1.590 and 1.628 Å, respectively, using the same aug-cc-pVTZ basis set. If all the electrons are correlated, the

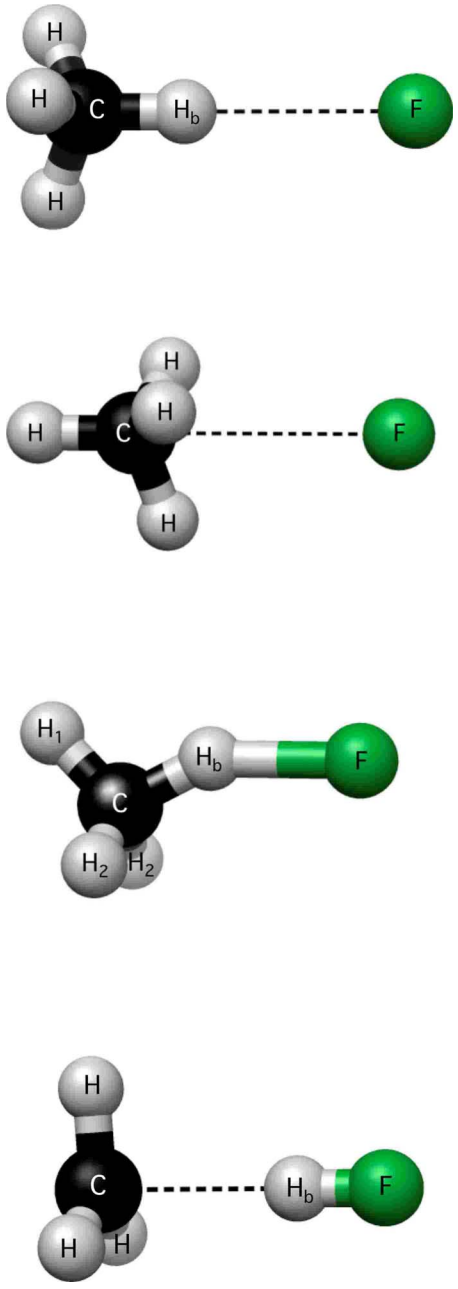

FIG. 2. (Color online) Equilibrium structures of the two $(CH_4\text{- - -F})_{vdW}$ as well as the $(CH_4\text{- -F})_{SP}$ and the $(CH_3\text{- - -HF})_{vdW}$ complexes from up to down, respectively.

former bond length of 1.628 Å decreases to 1.621 Å. Finally, it is important to emphasize that the C–H$_b$–F angle depends sensitively on the treatment of the electron correlation. All the FC-RMP2, the FC-UMP2, and the AE-UMP2 methods give a bond angle of 180° regardless the size of the basis. Furthermore, the saddle point structure is collinear even if the AE-UCCSD method is employed. Therefore, we can state that the triple excitations in the CC series are required to correctly describe the bent structure; since only the post-CCSD methods, e.g., UCCSD(T), provide bent C–H$_b$–F angle.

One-dimensional relaxed bending potentials along the C–H$_b$–F angle at UMP2 and UCCSD(T) levels are shown in Fig. 3. The four atoms H$_1$–C–H$_b$–F are in the C_s plane and H$_1$, and F can be in *cis* and *trans* positions. As shown in Fig. 3 the *trans* is the energetically favorable configuration. It is also important to note that the UCCSD(T) energies corresponding to the bent (C_s) and the collinear (C_{3v}) structures differ by only a few wavenumbers indicating that the saddle point structure is highly fluxional.

B. Van der Waals complex $(CH_3\text{- - -HF})_{vdW}$

The equilibrium structures of the reactant (CH_4), the products (CH_3 and HF), and the $(CH_3\text{- - -HF})_{vdW}$ complex are given in Table VII computed at different levels of theory. The vdWP complex has C_{3v} point-group symmetry even if the UCCSD(T) method is used for the optimizations. The best estimates for the bond lengths r(C–H), r(C–H$_b$), and r(H$_b$–F), see Fig. 2, are 1.078, 2.142, and 0.925 Å, respectively, while the bond angle α(H–C–H$_b$) is 93.1° obtained at the AE-UCCSD(T)/aug-cc-pCVQZ level of theory. For comparison the CH and HF equilibrium bond lengths in the free CH_3 and HF molecules are 1.077 and 0.917 Å, respectively, at the same level of theory. As these results show the structures of the monomers in the complex are very similar to the equilibrium geometries of the products. The D_{3h} point-group symmetry of the CH_3 unit is also just slightly compromised in the complex; since α(H–C–H$_b$) differs from 90° only by 3.1°. Unlike for the SP, in the case of the $(CH_3\text{- - -HF})_{vdW}$ complex, the MP2 methods give reasonable estimates for the equilibrium parameters. For example, the AE-UMP2/aug-cc-pCVQZ results for [r(C–H), r(C–H$_b$), r(H$_b$–F), and α(H–C–H$_b$)] are [1.073, 2.146, 0.926 Å, and 93.2°]. Furthermore, the differences between the results obtained with restricted or unrestricted methods are also smaller than the corresponding deviations in the case of the SP structure. The effect of the core electron correlation on the equilibrium geometry of $(CH_3\text{- - -HF})_{vdW}$ has also been found negligible.

C. Van der Waals complexes $(CH_4\text{- - -F})_{vdW}$

We found two vdW complexes in the entrance valley with C–H$_b$–F(second-order saddle point) and H–C–F(minimum) bond arrangements along the C_{3v} axis (see Fig. 2). In the case of the C–H$_b$–F bond arrangement one-dimensional potential energy curves as a function of the H$_b$–F separation are shown in Fig. 4. Test calculations showed that in the vdWR complex regions the F atom perturbs only slightly the equilibrium structure of the free CH_4, and the perturbation does not result in more than a 1–2 cm^{-1} effect on the dissociation energy of the corresponding vdWR complex. At the C–H$_b$–F vdWR region there are two electronic states, i.e., $^2A_1$ and ^2E (assuming C_{3v} symmetry), close to each other in energy. The equilibrium H$_b$–F distances (SO effects) are 2.482(+0.155) and 2.851 (+0.000) Å corresponding to the stationary points of the AE-UCCSD(T)/aug-cc-pCVQZ potentials of the $^2A_1$ and ^2E states, respectively. It is important to emphasize that the uncertainties of the equilibrium parameters are large, i.e., about ±0.1 Å, since an extremely high level of theory is required to describe this vdWR region accurately. The stationary points with C–H$_b$–F bond arrangement are below the F +$(CH_4)_{eq}$ asymptote by 40 and 73 cm^{-1} for the $^2A_1$ and ^2E

TABLE VI. Equilibrium structure of $(CH_4\text{- -}F)_{SP}$ and classical barrier height (V_{SP}, cm^{-1}) at different levels of theory [all the bond lengths (r) are in Å and all the bond angles (α) and the torsion angle (τ) are in degrees; see Fig. 2 for the notations].

Methods[a]	$r(CH_1)$	$r(CH_2)$	$r(CH_b)$	$r(H_bF)$	$\alpha(H_1CH_b)$	$\alpha(H_2CH_b)$	$\alpha(CH_bF)$	$\tau(H_2CH_bF)$	V_{SP}
FC-RMP2/aug-cc-pVDZ	1.096	1.096	1.139	1.424	106.9	107.0	179.5	120.0	1543
FC-RMP2/aug-cc-pVTZ	1.084	1.084	1.126	1.422	107.1	107.2	181.7	120.0	1491
FC-RMP2/aug-cc-pVQZ	1.083	1.082	1.124	1.424	106.9	107.2	173.9	120.0	1466
FC-UMP2/aug-cc-pVDZ	1.096	1.096	1.137	1.466	107.1	107.1	180.0	120.0	1204
FC-UMP2/aug-cc-pVTZ	1.084	1.084	1.124	1.460	107.3	107.3	180.1	120.0	1206
FC-UMP2/aug-cc-pVQZ	1.083	1.083	1.122	1.462	107.3	107.3	180.0	120.0	1186
AE-UMP2/aug-cc-pCVDZ	1.095	1.095	1.135	1.467	107.1	107.1	179.9	120.0	1153
AE-UMP2/aug-cc-pCVTZ	1.083	1.083	1.122	1.458	107.2	107.3	180.0	120.0	1249
AE-UMP2/aug-cc-pCVQZ	1.081	1.081	1.121	1.459	107.2	107.2	180.1	120.0	1230
FC-RCCSD(T)/aug-cc-pVDZ	1.102	1.101	1.126	1.606	107.3	108.0	163.1	119.9	199
FC-RCCSD(T)/aug-cc-pVTZ	1.089	1.088	1.114	1.590	107.4	108.1	162.4	119.9	246
FC-UCCSD(T)/aug-cc-pVDZ	1.102	1.101	1.124	1.641	107.2	108.3	153.4	119.8	110
FC-UCCSD(T)/aug-cc-pVTZ	1.090	1.088	1.112	1.628	107.3	108.3	152.5	119.8	139
AE-UCCSD(T)/aug-cc-pCVDZ	1.101	1.100	1.121	1.649	107.3	108.3	154.1	119.8	79
AE-UCCSD(T)/aug-cc-pCVTZ	1.088	1.087	1.111	1.621	107.2	108.3	152.3	119.8	186

[a]FC and AE denote frozen-core and all-electron computations, respectively.

states, respectively. In the H–C–F vdWR region the separation between the two electronic states is larger, i.e., the non-SO D_e values differs by about 150 cm^{-1} and unlike in the $C-H_b-F$ region (see Fig. 4), there is no crossing between the states. The C–F equilibrium distance (SO effect) is 2.940(+0.105) Å for the ground electronic state ($^2A_1$). This H–C–F vdW minimum is significantly deeper than the stationary point in the $C-H_b-F$ region; since the D_e value, including relatively large SO effect of −53 cm^{-1}, is 158 cm^{-1}. The summary of these results as well as more computational details are given in Table VIII.

D. Internal rotation

The possibility of the internal rotation of the CH_4 as a function of the position of the F atom may provide an interesting feature for the vibrational spectra of the complexes in the reactant channel. For example, Neumark[45] and coworkers have been using the $F^-–CH_4$ anion complex as precursor in photodetachment spectroscopy to probe the neutral system. In order to study this internal rotation the following model is considered. Let us suppose that the CH_4 unit is a spherical top and the starting structure has C_{3v} symmetry, where $C-H_b-F$ is collinear and the C–F separation is the sum of the $C-H_b$ and H_b-F equilibrium distances at the SP. The one-dimensional potential describing the internal rotation has been obtained as a function of the $F-C-H_b$ angle while the F atom goes around the CH_4 unit in the C_s plane with fixed C–F distance. This potential has been computed at the FC-UCCSD(T)/aug-cc-pVTZ level of theory and is shown in Fig. 5. Note that the energy of the collinear starting structure is above the SP energy by about 80 cm^{-1}; since the effects of $C-H_b-F$ bending, $C-H_b$ stretching, and $H-C-H_b$ tetrahedral angle distortion would result in energy decrease, with respect to the energy of the above-defined "model SP," of about 10, 20, and 50 cm^{-1}, respectively. A rotation to the *cis* direction by 109.5° corresponds to the H atom "substitution." As Fig. 5 shows this rotation is not hindered, since the $C-H_b-F$ collinear structure is the global maximum on this one-dimensional potential and the local minimum at 54.7° is below the collinear $C-H_b-F$ structure by about 390 cm^{-1}. Due to the fact that the C–F equilibrium separation in the H–C–F vdWR complex is close to the C–F distance at the SP the rotation by 180° provides a structure in the vdWR well with an energy below the $F+(CH_4)_{eq}$ dissociation limit by about 200 cm^{-1}. Furthermore, this relatively deep vdWR well can be accessed by a rotation of 70.5°, i.e., 180°–109.5°, on the *trans* half-circle of the C_s plane. The rotation between two equivalent vdWR complexes is slightly hindered since the barrier height between the two minima at 70.5° and 180° is about 40 cm^{-1} corresponding to the above-defined fixed C–F separation. Therefore, we speculate that the features of the photodetachment spectrum may correspond to the hindered rotor motion of the H–C–F vdWR complex. Further work to investigate this quantitatively is in progress.

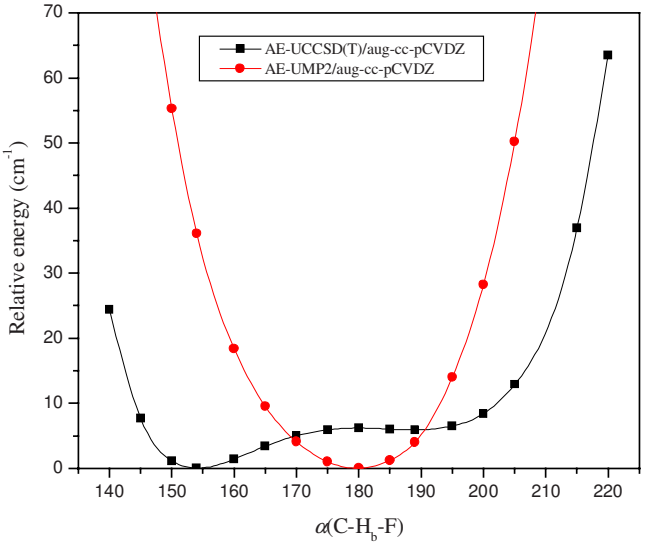

FIG. 3. (Color online) Bending potentials along the $C-H_b-F$ angle of $(CH_4\text{- -}F)_{SP}$ (see Fig. 2) at two different levels of theory. The curves were obtained using constrained optimizations.

TABLE VII. Equilibrium structures of the reactant, products, and the vdW complex $(CH_3\text{- - -}HF)_{vdW}$ and relative energies at different levels of theory [all the bond lengths (r) are in Å and the bond angles (α) are in degrees; see Fig. 2 for the notations].

	F+CH_4	$(CH_3\text{- - -}HF)_{vdW}(C_{3v})$					HF+$CH_3(D_{3h})$		
Methods[a]	r(CH)	r(CH)	$r(CH_b)$	$r(H_bF)$	$\alpha(HCH_b)$	D_e [b]	r(CH)	r(HF)	ΔH_e° [b]
FC-RMP2/aug-cc-pVDZ	1.098	1.089	2.187	0.932	93.1	1119	1.088	0.925	−11 127
FC-RMP2/aug-cc-pVTZ	1.086	1.077	2.139	0.930	93.0	1151	1.075	0.922	−11 592
FC-RMP2/aug-cc-pVQZ	1.085	1.075	2.142	0.927	92.8	1102	1.074	0.919	−11 929
FC-UMP2/aug-cc-pVDZ		1.089	2.191	0.932	93.5	1110	1.088		−11 115
FC-UMP2/aug-cc-pVTZ		1.077	2.144	0.930	93.5	1140	1.075		−11 554
FC-UMP2/aug-cc-pVQZ		1.075	2.146	0.927	93.3	1091	1.073		−11 889
AE-UMP2/aug-cc-pCVDZ	1.097	1.088	2.180	0.932	93.5	1149	1.086	0.924	−11 141
AE-UMP2/aug-cc-pCVTZ	1.085	1.075	2.143	0.929	93.4	1131	1.074	0.921	−11 517
AE-UMP2/aug-cc-pCVQZ	1.083	1.073	2.146	0.926	93.2	1084	1.072	0.918	−11 854
FC-RCCSD(T)/aug-cc-pVDZ	1.103	1.095	2.189	0.931	93.4	1140	1.093	0.924	−9 314
FC-RCCSD(T)/aug-cc-pVTZ	1.090	1.081	2.139	0.929	93.4	1172	1.079	0.921	−9 764
FC-RCCSD(T)/aug-cc-pVQZ	1.088	1.079	2.142	0.925	93.2	1111	1.078	0.918	−10 120
FC-UCCSD(T)/aug-cc-pVDZ		1.095	2.188	0.931	93.3	1142	1.093		−9 324
FC-UCCSD(T)/aug-cc-pVTZ		1.081	2.137	0.929	93.4	1174	1.080		−9 771
FC-UCCSD(T)/aug-cc-pVQZ		1.079	2.142	0.925	93.2	1114	1.078		−10 125
AE-UCCSD(T)/aug-cc-pCVDZ	1.101	1.093	2.177	0.931	93.3	1180	1.092	0.924	−9 317
AE-UCCSD(T)/aug-cc-pCVTZ	1.088	1.080	2.137	0.928	93.3	1162	1.078	0.920	−9 717
AE-UCCSD(T)/aug-cc-pCVQZ	1.087	1.078	2.142	0.925	93.1	1105	1.077	0.917	−10 077

[a]FC and AE denote frozen-core and all-electron computations, respectively.
[b]Dissociation energy (D_e) of $(CH_3\text{- - -}HF)_{vdW}$ and the vibrationless enthalpy of the reaction (ΔH_e°) are given in cm^{-1}.

V. VIBRATIONAL ENERGY LEVELS

ZPVEs and all the fundamental frequencies for CH_4 and $(CH_4\text{- -F})_{SP}$ as well as for $(CH_3\text{- - -}HF)_{vdW}$, CH_3, and HF are presented in Tables IX and X, respectively. The harmonic frequencies correspond to the fitted PES and for comparison FC-UCCSD(T)/aug-cc-pVTZ *ab initio* values are also given. For all the species except the SP variational vibrational calculations have also been performed. Unlike the harmonic fundamentals these variationally computed anharmonic frequencies of the reactant and the products allow direct comparison between theory and experiment. Since the variational solution of the vibrational Schrödinger equation provides vibrational energies corresponding to the given PES within spectroscopic accuracy, the differences between the computed and measured frequencies indicate the accuracy of the PES. The averaged absolute deviations between the calculated and experimental fundamentals are 9, 16, and 20 cm^{-1} for CH_4, CH_3, and HF, respectively.

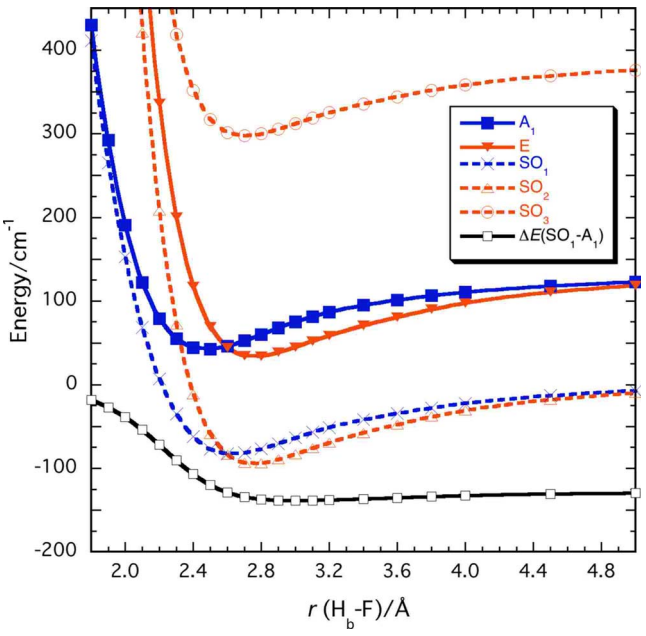

FIG. 4. (Color online) Potential energy curves of $CH_4\text{- - -}F$ as a function of the H_b–F distance (see Fig. 2) along the C_{3v} axis. These curves were computed at the frozen-core MRCI+Q/aug-cc-pVTZ level with the standard full-valence active space (the A_1 antibonding orbital of CH_4 was removed for the SO calculations), keeping the CH_4 unit at its equilibrium structure.

A. Saddle point $(CH_4\text{- -F})_{SP}$

The $(CH_4\text{- -F})_{SP}$ complex has a relatively low imaginary frequency of $357i$ cm^{-1} corresponding to an intermolecular stretching mode between CH_4 and F. Furthermore, $(CH_4\text{- -F})_{SP}$ has two low-lying fundamentals, $\omega_b(a')=40$ cm^{-1} and $\omega_b(a'')=117$ cm^{-1}, which correspond to intermolecular bending modes. The other nine fundamentals correspond to the vibrational modes of the CH_4 unit. The harmonic frequencies (all in cm^{-1}) of CH_4 are $\omega_4(t_2)=1329$, $\omega_2(e)=1569$, $\omega_1(a_1)=3032$, and $\omega_3(t_2)=3145$, whereas the corresponding fundamentals of $(CH_4\text{- -F})_{SP}$ are (1255, 1335, 1361), (1520, 1539), 2604, and (3070, 3185, 3203), respectively. The saddle point has a bent (C_s) structure; therefore, all the degenerate fundamentals of CH_4 are split as shown in parentheses. Note that, similar to the F^-–CH_4 anion complex,[43] the CH_b stretching fundamental, where H_b is connected to F, of $(CH_4\text{- -F})_{SP}$ is redshifted by about 400 cm^{-1} relative to the corresponding frequency of the free CH_4 molecule.

TABLE VIII. Equilibrium structures (Å) [the equilibrium distances at the AE UCCSD(T)/aug-cc-pCVQZ level for the C-H_b- - -F and the H-C- - -F complexes (see Fig. 2)] and dissociation energies (D_e,cm^{-1}) [single-point AE-UCCSD(T) calculations at the given non-SO equilibrium structures] of the vdW complexes in the entrance valley.

C_{3v} axes	C-H_b- - -F		H-C- - -F	
States	$^2A_1$	^2E	$^2A_1$	^2E
r(C–F)[r(H_b–F)]	3.572[2.482]	3.940[2.851]	2.940	3.504
$\Delta_{SO}r$(C–F)[$\Delta_{SO}r$(H_b–F)] [a]	+0.155[+0.155]	+0.000[+0.000]	+0.105	+0.000
r_{SO}(C–F)[r_{SO}(H_b–F)] [a]	3.727[2.637]	3.940[2.851]	3.045	3.504
	D_e	D_e	D_e	D_e
aug-cc-pCVTZ	90.2	92.1	238.1	84.1
aug-cc-pCVQZ	60.2	73.3	227.1	74.8
aug-cc-pCV5Z	42.4		211.0	
SO effect[b]	−2.9	+0.0	−53.1	+0.0
Final D_e values	39.5	73.3	157.9	74.8

[a]SO corrections to the bond lengths (see footnote b). The best estimates for the bond lengths were obtained as the sum of the nonrelativistic values and the SO corrections.
[b]Spin-orbit effect was computed with the Breit–Pauli operator in the interacting states approach (Ref. 35) at frozen-core MRCI+Q/aug-cc-pVTZ level using an active space of 15 valence electrons in 11 spatial orbitals, i.e., the A_1 antibonding orbital of CH_4 was removed from the full-valence active space.

B. Van der Waals complex $(CH_3$- - -$HF)_{vdW}$

Variational vibrational calculations have been performed in full (12) dimensions using our global PES and the equilibrium geometry of $(CH_3$- - -$HF)_{vdW}$ as a reference structure. Since the $(CH_3$- - -$HF)_{vdW}$ complex is a weakly bonded extremely floppy system several MM computations have been carried out in order to check the convergence of the vibrational energy levels. First, calculations were performed using 2MR, 3MR, 4MR, and 5MR of the PES employing the same $[7_7 5_8 3_6 2_5 1_5]$ basis of 8544 functions. The absolute average deviations between the fundamentals obtained with 5MR and the 2MR, 3MR, and 4MR results are 204, 10, and 2 cm^{-1}, respectively. Due to the fact that the 4MR and 5MR give the same energies within 1–2 cm^{-1}, it is not worth using the computationally much more expensive 5MR with a more complete basis set. In the second part of the convergence test MM calculations were performed using 4MR with systematically increased basis set size. This convergence study started with the modest $[4_4 3_4 2_4 1_4]$ basis, and the average $\delta[5_5 4_5 3_5 2_5 1_5]$, $\delta[6_6 5_6 4_6 3_6 2_6]$, and $\delta[7_7 6_7 4_7 3_6 2_6]$ absolute increments in the fundamentals with respect to the preceding basis are 70, 8, and 4 cm^{-1}, respectively. Note that the $\upsilon_4(e)=545$ cm^{-1} degenerate level has the slowest convergence behavior among the fundamentals and without this frequency the averaged $\delta[7_7 6_7 4_7 3_6 2_6]$ increment drops to 2 cm^{-1}. This convergence study predicts that the largest basis provides converged vibrational fundamentals within a few wavenumbers. Therefore, the $[7_7 6_7 4_7 3_6 2_6]$ basis of 20688 functions has been employed to compute our final results.

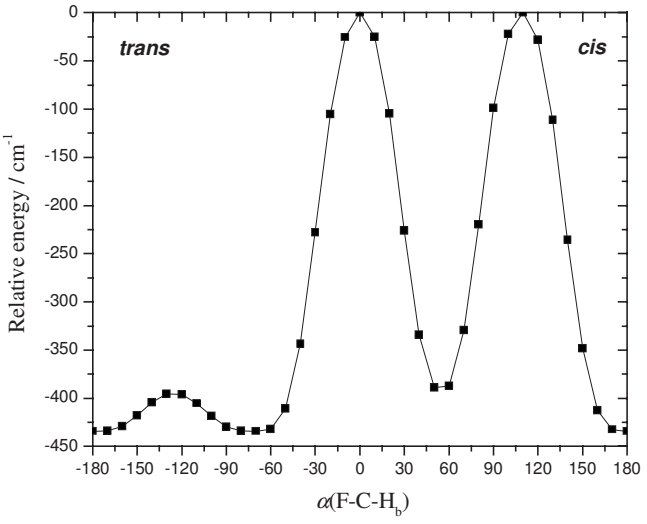

FIG. 5. Potential energy curve along the F–C–H_b angle in the C_s plane involving H_1, C, H_b, F (see. Fig. 2) computed at the frozen-core UCCSD(T)/aug-cc-pVTZ level of theory. The CH_4 unit is a spherical top with CH distance of 1.090 Å and the C–F separation is fixed at 2.738 Å. The relative energies of the $(CH_4$- -F$)_{SP}$ and the F+$(CH_4)_{eq}$ dissociation limit are at −82 and −221 cm^{-1} on the energy scale of this figure, respectively.

Since the $(CH_3$- - -$HF)_{vdW}$ complex is composed of weakly interacting CH_3 and HF molecules, 7(6+1) of the 12 fundamentals of the complex correspond to the frequencies of the monomers. The computed anharmonic fundamentals (all in cm^{-1}) of the free CH_3 are $\upsilon_4(a_2'')=598$, $\upsilon_2(e')=1380$, $\upsilon_1(a_1')=2983$, and $\upsilon_3(e')=3144$, whereas the corresponding frequencies of the vdWP complex are 707, 1407, 3034, and 3177 cm^{-1}, respectively. In the case of the HF stretching of the complex there is a significant difference between the UCCSD(T)/aug-cc-pVTZ *ab initio* harmonic frequency (3940 cm^{-1}) and the harmonic fundamental corresponding to the PES (4050 cm^{-1}). Therefore, our best estimate for this fundamental is 3940+(3896–4050)=3786 cm^{-1}, where in parenthesis the anharmonicity is calculated using the MM result. This computed HF fundamental is in good agreement with the recently measured vibrational band of 3797 cm^{-1} by infrared laser spectroscopy in helium nanodroplets.[46] The HF stretching of the complex is significantly redshifted relative to the variationally computed vibrational fundamental of

TABLE IX. ZPVEs and all the fundamentals (in cm^{-1}) for CH_4 and the saddle point $(CH_4\text{- -F})_{SP}$.

CH_4				$(CH_4\text{- -F})_{SP}$	
	ω [a]	v [b]	Expt.[c]		ω [a]
ZPVE	9796(9834)	9655		$ZPVE_{SP}$	9615(9839)
				$\omega_s(a')$	357*i*(246*i*)
				$\omega_b(a')$	40(277)
				$\omega_b(a'')$	117(344)
$v_4(t_2)$	1329(1351)	1302	1311	$\omega_4(a')$	1255(1289)
				$\omega_6(a'')$	1335(1290)
				$\omega_6(a')$	1361(1313)
$v_2(e)$	1569(1574)	1529	1533	$\omega_2(a'')$	1520(1545)
				$\omega_2(a')$	1539(1569)
$v_1(a_1)$	3032(3028)	2903	2917	$\omega_1(a')$	2604(2604)
$v_3(t_2)$	3145(3146)	3012	3020	$\omega_3(a')$	3070(3078)
				$\omega_5(a')$	3185(3177)
				$\omega_5(a'')$	3203(3193)

[a]Harmonic frequencies corresponding to the PES, while the frozen-core UCCSD(T)/aug-cc-pVTZ *ab initio* results are given in parentheses. In the case of the $(CH_4\text{- -F})_{SP}$ frequencies, especially for the low-lying ones, the *ab initio* values have significant uncertainties due to uncertainties in the numerical Hessian calculation.
[b]VCI energies were computed with 4MR using the $[7_7 6_7 5_7 3_6 2_6]$ basis of 6406 functions.
[c]Experimental levels for CH_4 were taken from Ref. 50.

the HF monomer (3941 cm^{-1}). The low-lying frequencies of the complex, $v_s(a_1)=138$ cm^{-1} and $v_b(e)=275$ cm^{-1}, correspond to the intermolecular stretching and bending modes, respectively. Note that the $v_b(e)$ mode is highly anharmonic; since its harmonic frequency is only 132 cm^{-1}.

VI. HIGHLY ACCURATE THERMOCHEMISTRY

Accurate SP barrier and ground state vibrationally adiabatic barrier heights (V_{SP} and V_{VAGS}), dissociation energy of the $(CH_3\text{- - -HF})_{vdW}$ complex (D_e and D_0), and enthalpy of the title reaction (ΔH_e° and ΔH_0°) have been determined using the FPA approach. Single-point electron energy calculations have been performed for the species, F, CH_4, HF, CH_3, $(CH_4\text{- -F})_{SP}$, and $(CH_3\text{- - -HF})_{vdW}$. In the case of the barrier height calculations the AE-UCCSD(T)/aug-cc-pCVTZ reference structures have been used, while the dissociation energy and reaction enthalpy have been obtained using the AE-UCCSD(T)/aug-cc-pCVQZ equilibrium structures. The FPA results for the vibrationless AE nonrelativistic BO values of V_{SP}, D_e, and ΔH_e° are presented in Tables XI–XIII, respectively. The summary of the FPA including the auxiliary corrections as well as the final V_{VAGS}, D_0, and ΔH_0° values is given in Table XIV.

A. All-electron nonrelativistic Born–Oppenheimer V_{SP}, D_e, and ΔH_e° values

Both for V_{SP} and D_e the aug-cc-pCV*X*Z basis sets have been employed, where $X=2-5(6)$ up to the AE-UCCSD(T)(RMP2) method. Electron correlation energies have also been taken into account beyond the AE-UCCSD(T) level by performing AE-UCCSDT and AE-UCCSDT(Q) calculations using the aug-cc-pCVDZ basis set. For the determination of ΔH_e° the aug-cc-pCV6Z basis set has been used up to the UCCSD(T) level and more accurate computations have been performed beyond the UCCSD(T) level as well.

TABLE X. ZPVEs and vibrational frequencies (in cm^{-1}) for the product vdW complex $(CH_3\text{- - -HF})_{vdW}$ and the products (CH_3 and HF).

$(CH_3\text{- - -HF})_{vdW}$			CH_3				HF			
	ω [a]	v [b]		ω [a]	v [b]	Expt.[c]		ω [a]	v [b]	Expt.[c]
ZPVE	9248(9172)	9180	ZPVE	6486(6518)	6424		ZPVE	2049(2062)	2 033	
$v_{HF}(a_1)$	4050(3940)	3896[d]					v_1	4098(4124)	3 941	3 961
$v_s(a_1)$	119(140)	138					v_2	8196(8248)	7 725	7 751
$v_b(e)$	132(136)	275					v_3	12294(12372)	11 354	11 373
$v_4(e)$	459(422)	545					v_4	16392(16496)	14 825	14 832
$v_4(a_1)$	671(637)	707	$v_4(a_2'')$	508(496)	598	606				
$v_2(e)$	1401(1421)	1407	$v_2(e')$	1407(1419)	1380	1397				
$v_3(a_1)$	3113(3103)	3034	$v_1(a_1')$	3090(3114)	2983	3004				
$v_3(e)$	3280(3283)	3177	$v_3(e')$	3280(3294)	3144	3161				

[a]Harmonic frequencies corresponding to the PES, while the frozen-core UCCSD(T)/aug-cc-pVTZ *ab initio* results are given in parentheses.
[b]For $(CH_3\text{- - -HF})_{vdW}$ and CH_3 VCI energies were computed with 4MR using the bases $[7_7 6_7 4_7 3_6 2_6]$ of 20 688 and $[7_7 6_7 5_7 3_6 2_6]$ of 1319 functions, respectively. In the case of HF converged anharmonic vibrational levels were obtained by a one-dimensional discrete variable representation code.
[c]Experimental levels for CH_3 and HF were taken from Refs. 51 and 52, respectively.
[d]Our best estimate for the anharmonic $v_{HF}(a_1)$ is $3940+(3896-4050)=3786$ cm^{-1}.

TABLE XI. Focal-point analysis of the AE nonrelativistic Born–Oppenheimer classical barrier height (V_{SP},cm^{-1}) of F+CH$_4$→(CH$_4$- -F)$_{SP}$. [The results correspond to the structures optimized at the AE UCCSD(T)/aug-cc-pCVTZ level of theory. For the AE correlation methods, the symbol δ denotes the increments in V_{SP} with respect to the preceding level of theory. Brackets signify assumed, nonextrapolated, increments from smaller basis set results.]

	V_{SP}[ROHF]	δ[RMP2]	δ[UCCSD]	δ[UCCSD(T)]	δ[UCCSDT]	δ[UCCSDT(Q)]	V_{SP}
aug-cc-pCVDZ	3131.4	−2144.1	−574.8	−337.0	−50.4	−34.9	−9.9
aug-cc-pCVTZ	3243.5	−2187.2	−470.9	−399.3	[−50.4]	[−34.9]	100.8
aug-cc-pCVQZ	3262.5	−2228.7	−462.2	−420.1	[−50.4]	[−34.9]	66.2
aug-cc-pCV5Z	3289.0	−2219.1	−457.3	−426.5	[−50.4]	[−34.9]	100.8
aug-cc-pCV6Z	3291.5	−2216.3	[−457.3]	[−426.5]	[−50.4]	[−34.9]	106.1
CBS[a]	3292.0	−2212.4	−452.1	−433.2	−50.4	−34.9	109.0

[a]The complete basis set (CBS) ROHF energy and the RMP2, UCCSD, and UCCSD(T) electron correlation energies were calculated using two-parameter extrapolation formulas given in Eqs. (2) and (3), respectively. Only the best two energies were included in the extrapolations.

The ROHF energies have been extrapolated to determine the ROHF CBS limit, E_{CBS}^{HF}, employing a two-parameter exponential formula,[47]

$$E_X^{HF} = E_{CBS}^{HF} + a(X+1)e^{-9\sqrt{X}}, \tag{2}$$

where E_X^{HF} is the ROHF energy obtained by the corresponding aug-cc-pCVXZ basis set. The extrapolations have been performed for all the individual species using the X=5,6 values. Since the ROHF energies converge exponentially the absolute differences between the ROHF CBS limits of the V_{SP}, D_e, and ΔH_e° values and the corresponding ROHF/aug-cc-pCV6Z results are only 0.5, 0.4, and 0.1 cm^{-1}, respectively.

The electron correlation energies, E_X, have been extrapolated using a two-parameter polynomial formula[48]

$$E_X = E_{CBS} + bX^{-3}, \tag{3}$$

where E_{CBS} is the CBS limit of the correlation energy. Due to the fact that Eq. (3) is an asymptotic formula, the best estimates for the CBS limits can be obtained by using the best two energies in the extrapolations. For V_{SP} and D_e the aug-cc-pCV5Z(aug-cc-pCV6Z) and CBS (δ[RMP2], δ[UCCSD], δ[UCCSD(T)]) increments with respect to the preceding level of theory deviate by (6.7(3.9),5.2,6.7) cm^{-1} and (15.8(9.2),1.8,0.5) cm^{-1}, respectively. In the case of ΔH_e° the corresponding absolute differences between the aug-cc-pCV6Z and CBS increments are (36.5,8.9,3.8) cm^{-1}.

The contribution of the electron correlation energies to the final results are extremely large; since the CBS ROHF values and the effects of all the single and double, all the triple, and the perturbative (or for ΔH_e° all the) quadruple excitations are (3292.0,−2664.5,−483.6, and−34.9) cm^{-1}, (395.3, +552.0,+117.3, and +1.8) cm^{-1} and (−4150.1, −5625.5,−383.4, and−26.6) cm^{-1}, in order, for V_{SP}, D_e, and ΔH_e°, respectively. The effects of the neglected excitations beyond the quadruples are likely to be a few wavenumbers and less than 1 cm^{-1} on the value of D_e. It is important to emphasize that both the HF and MP2 methods and even CCSD give unreasonable estimates for all three quantities. For example, the MP2 method overestimates the V_{SP} value by an order of magnitude. Our best estimate for the AE nonrelativistic BO V_{SP}, D_e, and ΔH_e° values are 109.0, 1066.4, and −10 185.7 cm^{-1}, respectively.

B. Scalar relativistic effects

Scalar relativistic corrections have been computed at the AE-UCCSD(T)/aug-cc-pCVQZ level of theory using the Douglas–Kroll relativistic one-electron integrals. The scalar relativistic effects on the values of V_{SP}, D_e, and ΔH_e° are +3.2, −0.1, and +61.2 cm^{-1}, respectively. These corrections are converged within 1–2 cm^{-1}; since the corresponding

TABLE XII. Focal-point analysis of the AE nonrelativistic Born−Oppenheimer dissociation energy (D_e,cm^{-1}) of (CH$_3$- - -HF)$_{vdW}$. [The results correspond to the structures optimized at the AE UCCSD(T)/aug-cc-pCVQZ level of theory. For the AE correlation methods, the symbol δ denotes the increments in D_e with respect to the preceding level of theory. Brackets signify assumed, nonextrapolated, increments from smaller basis set results.]

	D_e[ROHF]	δ[RMP2]	δ[UCCSD]	δ[UCCSD(T)]	δ[UCCSDT]	δ[UCCSDT(Q)]	D_e
aug-cc-pCVDZ	433.9	+722.0	−86.9	+110.4	+3.8	+1.8	1185.1
aug-cc-pCVTZ	429.9	+711.4	−91.7	+112.1	[+3.8]	[+1.8]	1167.3
aug-cc-pCVQZ	408.8	+685.6	−102.1	+112.5	[+3.8]	[+1.8]	1110.5
aug-cc-pCV5Z	397.7	+673.3	−103.7	+113.0	[+3.8]	[+1.8]	1085.8
aug-cc-pCV6Z	395.7	+666.7	[−103.7]	[+113.0]	[+3.8]	[+1.8]	1077.2
CBS[a]	395.3	+657.5	−105.5	+113.5	+3.8	+1.8	1066.4

[a]The CBS ROHF energy and the RMP2, UCCSD, and UCCSD(T) electron correlation energies were calculated using two-parameter extrapolation formulas given in Eqs. (2) and (3), respectively. Only the best two energies were included in the extrapolations.

TABLE XIII. Focal-point analysis of the AE nonrelativistic Born−Oppenheimer vibrationless enthalpy (ΔH_e°,cm^{-1}) of the F+CH$_4$→HF+CH$_3$ reaction. [The results correspond to the structures optimized at the AE UCCSD(T)/aug-cc-pCVQZ level of theory. For the AE correlation methods, the symbol δ denotes the increments in ΔH_e° with respect to the preceding level of theory. Brackets signify assumed, nonextrapolated, increments from smaller basis set results.]

	ΔH_e°[ROHF]	δ[RMP2]	δ[UCCSD]	δ[UCCSD(T)]	δ[UCCSDT]	δ[UCCSDT(Q)]	δ[UCCSDTQ]	ΔH_e°
aug-cc-pCVDZ	−4048.1	−7103.8	+1980.9	−150.8	−1.7	−57.2	+6.0	−9374.6
aug-cc-pCVTZ	−4145.9	−7394.9	+2198.9	−373.2	+30.1	−32.6	[+6.0]	−9711.7
aug-cc-pCVQZ	−4164.4	−7718.9	+2205.0	−398.6	[+30.1]	[−32.6]	[+6.0]	−10073.5
aug-cc-pCV5Z	−4150.0	−7804.6	+2226.9	−407.0	[+30.1]	[−32.6]	[+6.0]	−10131.3
aug-cc-pCV6Z	−4150.0	−7831.2	+2233.3	−409.7	[+30.1]	[−32.6]	[+6.0]	−10154.2
CBS[a]	−4150.1	−7867.7	+2242.2	−413.5	+30.1	−32.6	+6.0	−10185.7

[a]The CBS ROHF energy and the RMP2, UCCSD, and UCCSD(T), electron correlation energies were calculated using two-parameter extrapolation formulas given in Eqs. (2) and (3), respectively. Only the best two energies were included in the extrapolations.

AE-UCCSD(T)/aug-cc-pCVTZ results are +3.0, −0.7, and +60.0 cm^{-1}, in order. The effect (−0.1 cm^{-1}) on the value of D_e is negligible, but the correction of +3.2 cm^{-1} is not negligibly small, since it is about 2% of the nonrelativistic V_{SP}. The scalar relativistic effect (+61.2 cm^{-1}) is largest for ΔH_e°, although it is only 0.6% of the nonrelativistic ΔH_e°. Due to the high-level of theory employed for the FPA of ΔH_e°, this relativistic correction is important in order to achieve the accuracy sought in this study.

C. Spin-orbit coupling effects

The effect of the SO coupling is defined as the difference between energies of the lowest SO state and the average ground state obtained by nonrelativistic computations. These SO effects are negligibly small for CH_4, CH_3, HF, and $(CH_3\text{- - -}HF)_{vdW}$. Therefore, the SO effect on the value of D_e is 0.0 cm^{-1}. However, the ground electronic state of the F atom is split by an experimental value of 404.1 cm^{-1} to SO states $^2P_{3/2}$ (SO ground state) and $^2P_{1/2}$. The computed SO coupling effect shows that the energy of the $^2P_{3/2}$ state is below the spin-orbit averaged state (^2P) by 131.5 cm^{-1}, and the computed SO coupling (394.3 cm^{-1}) is in good agreement with experiment. Thus, this effect shifts the ΔH_e° value by +131.5 cm^{-1}.

In the entrance channel of the F+CH$_4$ reaction, the SO effect almost vanishes at $r(H_b\text{–}F) < 1.5$ Å, the absolute value increases from 1.5 to 3.0 Å, and above 3.0 Å the effect tends to its asymptotic value (−131.5 cm^{-1}). The SO states and the SO effect for $CH_4\text{- - -}F$ are shown in Fig. 4 as a function of the H_b–F separation. At the saddle point the computed SO effect is −8.1 cm^{-1}, thus the effect on the value of V_{SP} is +123.4 cm^{-1}. It is important to emphasize that these SO coupling effects are not negligible especially in the case of the V_{SP} value, where this effect has the same order of magnitude as the nonrelativistic barrier height.

D. Diagonal Born–Oppenheimer corrections

The DBOCs have been computed at the ROHF(UHF)/aug-cc-pVTZ level and the corrections to the V_{SP}, D_e, and ΔH_e° values are +5.3(+9.7), +0.1(+2.1), and −11.9(−10.0) cm^{-1}, respectively. The difference between the ROHF and UHF results indicates a significant uncertainty in these DBOC values but this is negligible with respect to other source of errors. Furthermore, these relatively small DBOC corrections predict that the neglected so-called nonadiabatic effects do not compromise the accuracy of the final results.

E. Zero-point vibrational energy corrections

The ZPVE values of all the species are presented in Tables IX and X. The harmonic ZPVE corrections for the barrier height are −181, −267, and +5 cm^{-1} based on the PES, FC-UCCSD(T)/aug-cc-pVDZ, and FC-UCCSD(T)/aug-cc-pVTZ levels of theory, respectively. Therefore, it is clear that this value has a large uncertainty and we have chosen the correction of +5 cm^{-1}. The D_0 and ΔH_0° values can be calculated by utilizing the variationally computed fully anharmonic ZPVEs of CH_4, $(CH_3\text{- - -}HF)_{vdW}$, HF, and CH_3. In the case of the dissociation energy, the best estimate for the ZPVE correction is (−592)+(−723)−(−713)= −602 cm^{-1}, where the harmonic FC-UCCSD(T)/aug-cc-pVTZ, anharmonic MM, and harmonic PES relative ZPVEs are given in parentheses, respectively. For the reaction enthalpy the harmonic ZPVE corrections corresponding to the

TABLE XIV. Summary of the focal-point analysis results including the effects of the scalar relativity (Rel.) and the SO couplings, DBOC, and ZPVE corrections (all in cm^{-1}) for the barrier height and enthalpy of the F+CH$_4$→HF+CH$_3$ reaction as well as for the dissociation energy of $(CH_3\text{- - -}HF)_{vdW}$.

	Barrier height[a]	Dissociation energy[b]	Reaction enthalpy[b]
Hartree–Fock[c]	3292	395	−4150
Correlation[c]	−3183	+671	−6036
Rel.[d]	+3	+0	+61
SO[e]	+123	+0	+132
DBOC[f]	+5	+0	−12
V_{SP} D_e ΔH_e°	240	1066	−10 005
ZPVE[g]	+5	−602	−1198
V_{VAGS} D_0 ΔH_0°	245	464	−11 203

[a]The results correspond to the structures optimized at the AE-UCCSD(T)/aug-cc-pCVTZ level of theory.
[b]The results correspond to the structures optimized at the AE-UCCSD(T)/aug-cc-pCVQZ level of theory.
[c]See Tables XI–XIII.
[d]Douglas–Kroll relativistic corrections computed at the AE-UCCSD(T)/aug-cc-pCVQZ level of theory.
[e]See footnote b of Table VIII.
[f]DBOCs computed at the ROHF/aug-cc-pVTZ level of theory.
[g]Variationally computed anharmonic ZPVE corrections for D_0 and ΔH_0° and harmonic value for V_{VAGS} (see Sec. VI E).

PES (-1261 cm^{-1}) and the FC-UCCSD(T)/aug-cc-pVTZ level (-1254 cm^{-1}) are in good agreement, thus the uncorrected anharmonic MM ZPVE correction (-1198 cm^{-1}) has been employed to calculate ΔH_0°.

F. Thermal correction to the enthalpy of the reaction

The enthalpy of a reaction is usually defined at 298.15 K. Therefore, the ΔH_0° value, which corresponds to 0 K, needs to be converted to 298.15 K. The enthalpy of a reaction at a nonzero temperature (ΔH_T°) can be calculated as

$$\Delta H_T^\circ = \Delta H_0^\circ + \Delta H_{\mathrm{el}}(T) + \Delta H_{\mathrm{trans}}(T) + \Delta H_{\mathrm{vib}}(T) + \Delta H_{\mathrm{rot}}(T), \quad (4)$$

where $\Delta H_{\mathrm{el}}(T)$, $\Delta H_{\mathrm{trans}}(T)$, $\Delta H_{\mathrm{vib}}(T)$, and $\Delta H_{\mathrm{rot}}(T)$ are the temperature-dependent electronic, translational, vibrational, and rotational enthalpy changes, respectively. In the case of the $F+CH_4 \rightarrow HF+CH_3$ reaction $\Delta H_{\mathrm{trans}}(T)=0$ and $\Delta H_{\mathrm{el}}(T)=0$ if the SO coupling is neglected. Employing the classical rigid-rotor approximation $\Delta H_{\mathrm{vib}}(T)=0$ and $\Delta H_{\mathrm{rot}}(T)=(RT+3/2\ RT-3/2\ RT)=RT$, where the terms in parenthesis are the classical rotational energies of HF, CH_3, and CH_4, respectively. Thus, at 298.15 K the value of $\Delta H_{\mathrm{rot}}(T)$ is 207 cm^{-1}, which is the classical nonrelativistic thermal correction to the enthalpy of the reaction. In this study we do not use the classical approach, but the vibrational and rotational enthalpy contributions are computed via direct summation over the vibrational and rotational energies, respectively. The vibrational partition functions at 298.15 K can be obtained within 0.1 cm^{-1} by employing all the vibrational energy levels in the direct summation up to 3000 cm^{-1} above the ZPVE. Utilizing the variationally computed vibrational energies $\Delta H_{\mathrm{vib}}(T=298.15)=[0(HF)+38(CH_3)-9(CH_4)]=29$ cm^{-1}. Due to the fact that CH_3 has a low-lying fundamental (598 cm^{-1}) corresponding to the umbrella motion, the vibrational enthalpy contribution is not negligible. Direct summations over the rigid-rotor eigenenergies result in $\Delta H_{\mathrm{rot}}(T=298.15)=[200(HF)+309(CH_3)-309(CH_4)]=200$ cm^{-1}. Since the rotational constants of CH_3 (9.5 and 4.8 cm^{-1}) and CH_4 (5.3 cm^{-1}) are relatively small the rotational enthalpies of both the molecules are close to the classical value (311 cm^{-1}). However, HF has a relatively large rotational constant (20.8 cm^{-1}), thus the rotational enthalpy of HF is below the classical value by 7 cm^{-1}. Finally, since the electronic ground state of the F atom is split by 394 cm^{-1} due to the effect of the SO coupling, the $\Delta H_{\mathrm{el}}(T=298.15)=-27$ cm^{-1}. Summing the electronic, vibrational, and rotational enthalpy contributions, we arrive to our best estimate to the thermal correction for the title reaction, which is $-27+29+200=+202$ cm^{-1} at 298.15 K.

G. Final thermochemical quantities

The final ($V_{\mathrm{SP}}, D_e, \Delta H_e^\circ$) values are obtained by summing the AE nonrelativistic BO results (109, 1066, $-10\,186$ cm^{-1}), the scalar relativistic corrections ($+3, 0, +61$ cm^{-1}), the SO effects ($+123, 0, +132$ cm^{-1}), and the DBOCs ($+5, 0, -12$ cm^{-1}). Thus, the final vibrationless relativistic non-BO V_{SP}, D_e, and ΔH_e° values are 240 ± 40, 1070 ± 10, and -10000 ± 50 cm^{-1}, respectively. Adding the ZPVE corrections ($+5, -602, -1198$ cm^{-1}) to the vibrationless values results in the V_{VAGS}, D_0, and ΔH_0° values of 245 ± 200, 460 ± 50, and $-11\,200\pm80$ cm^{-1}, respectively. Finally, employing the thermal enthalpy correction ($+202$ cm^{-1}), we arrive to our best ΔH_{298}° value of $-11\,000\pm80$ cm^{-1}.

VII. QUASICLASSICAL TRAJECTORY CALCULATIONS

QCT calculations have been performed based on the new global PES in order to study the dynamics of the $F+CH_4 \rightarrow HF(v,J)+CH_3$ reaction. The internal energy of CH_4 was set to the harmonic ZPVE value, unless otherwise noted, by randomly distributing the harmonic ground state vibrational energy in the normal mode phase space. After the random sampling of the normal coordinates and momenta, the normal modes were transformed to the Cartesian coordinate system. The angular momentum of CH_4 was set to zero. The initial distance of the F atom from the center of the mass of the CH_4 molecule was $\sqrt{x^2+b^2}$, where b is the impact parameter and x was set to 10 bohr unless otherwise noted. The orientation of F was randomly rotated with respect to the CH_4 unit and b was scanned from 0 to $b_{\max}$ with a step size of 0.5 or 1.0 bohr. The parameter $b_{\max}$ is the maximum value of b where the required products are obtained. All the trajectories were integrated using 0.0726 fs integration step. Most of the trajectories were propagated for a maximum of 20 000 time steps (1452 fs).

A. HF rovibrational distributions

In order to simulate the $HF(v,J)$ product state distributions measured by Harper *et al.*,[11] we set the relative translational energy of F and CH_4 to the experimental collision energy of 630 cm^{-1} (1.8 kcal/mol). At this collision energy $b_{\max}$ was found to be 7 bohr. Thus, trajectories at impact parameters $b_n=0.5n$, where $n=0,1,\ldots,n_{\max}(14)$, have been calculated. The average probability of each rovibrational state is obtained as

$$\langle P_{v,J}\rangle = \sum_{n=1}^{n_{\max}} [b_n - b_{n-1}][b_n P_{v,J}(b_n) + b_{n-1}P_{v,J}(b_{n-1})]/b_{\max}^2, \quad (5)$$

where $P_{v,J}(b)$ is the probability of the rovibrational state (v,J) at the given value of b. For each impact parameter 5000 trajectories have been calculated, thus the total number of trajectories is 75 000 [70 000, since $P_{v,J}(0)$ has zero weight in Eq. (5)].

The vibrational and rotational quantum numbers have been assigned for the product HF as follows. First, the classical angular momentum j of HF was calculated using the final Cartesian coordinates and velocities. The quantum number J was obtained from the quantum mechanical expression $j=\sqrt{J(J+1)}$ by rounding J to the nearest integer value. Second, all the relevant rovibrational energy levels ($E_{v,J}$) of the HF molecule were computed variationally using a one-dimensional cut of our global PES. The vibrational quantum

TABLE XV. The HF(v,J) rotational-vibrational distributions (%) at collision energy of 630 cm^{-1}.

	$v=0$			$v=1$			$v=2$			$v=3$			$v=4$		
J	All[a]	Const.[b]	Expt.[c]	All[a]	Const.[b]	Expt.[c]	All[a]	Const.[b]	Expt.[c]	All[a]	Const.[b]	Expt.[c]	All[a]	Const.[b]	Expt.[c]
0	0.0	0.0		0.1	0.2	0.5	2.4	3.8	4.5	2.5	2.3	1.6	0.1	0.0	
1	0.0	0.0	2.3	0.3	0.5	1.6	8.8	13.7	10.5	9.0	7.0	3.3	0.4	0.0	
2	0.0	0.0	1.8	0.6	1.0	1.2	9.1	13.6	12.5	7.8	4.6	2.9	0.4	0.0	
3	0.0	0.0	−1.1	0.7	1.1	1.1	7.3	10.2	12.1	5.0	2.2	1.9	0.4	0.0	
4	0.0	0.0	−1.5	0.7	1.2	1.5	5.6	7.4	9.9	3.4	0.7	0.6	0.2	0.0	
5	0.0	0.0	−0.2	0.5	0.8	1.8	3.5	4.5	6.8	2.4	0.4	0.3	0.1	0.0	
6	0.0	0.0	0.5	0.5	0.9	1.4	2.7	3.3	4.1	1.7	0.2	0.2	0.0	0.0	
7	0.0	0.0	0.8	0.6	1.0	1.6	3.1	3.7	2.6	1.1	0.1	0.0	0.0	0.0	
8	0.0	0.0	0.0	0.9	1.4	2.5	2.5	2.7	1.6	0.8	0.0		0.0	0.0	
9	0.0	0.0	1.6	0.8	1.2	1.5	2.3	2.1	1.2	0.5	0.0		0.0	0.0	
10	0.0	0.0	−0.2	0.9	1.4	1.6	1.7	1.3	0.4	0.4	0.0		0.0	0.0	
11	0.0	0.0	0.1	0.8	1.2	0.9	1.2	0.8	0.3	0.3	0.0		0.0	0.0	
12	0.0	0.0	−0.6	0.6	0.8	1.0	1.0	0.5	0.2	0.1	0.0		0.0	0.0	
13	0.0	0.0	0.3	0.6	0.8	0.7	0.5	0.2	0.0	0.0	0.0		0.0	0.0	
14	0.0	0.0	0.2	0.4	0.5		0.4	0.0	0.0	0.0	0.0		0.0	0.0	
15	0.0	0.0		0.4	0.3		0.3	0.0		0.0	0.0		0.0	0.0	
16	0.0	0.0		0.2	0.1		0.1	0.0		0.0	0.0		0.0	0.0	
17	0.0	0.0		0.3	0.1		0.1	0.0		0.0	0.0		0.0	0.0	
18	0.0	0.0		0.2	0.1		0.1	0.0		0.0	0.0		0.0	0.0	
19	0.0	0.0		0.2	0.0		0.0	0.0		0.0	0.0		0.0	0.0	
20	0.0	0.0		0.1	0.0		0.0	0.0		0.0	0.0		0.0	0.0	
ΣJ	0.1	0.1	3.8	10.6	14.6	18.9	52.5	67.8	66.7	35.0	17.5	10.6	1.8	0.0	

[a]QCT results considering all the trajectories.
[b]QCT results without the trajectories that resulted in CH_3 product with internal energy less than its ZPVE.
[c]Experimental results taken from Ref. 11.

number v for HF was obtained by minimizing the formula $|E_{v,J}-E_{\text{int}}|$ with respect to v, where E_{int} is the internal, i.e. rovibrational, energy of the HF molecule and J is the previously calculated rotational quantum number.

According to quantum mechanics molecules vibrate even at 0 K and have nonzero vibrational ground state energy. However, due to the fact that QCT propagates the nuclei using classical mechanics, the reactive trajectories can result in products having less vibrational energy than the corresponding quantum mechanical ZPVE. In the present study almost all of the product HF molecules are vibrationally excited and none of them have less vibrational energy than the ZPVE of HF. However, the reaction produces a large fraction of vibrationally nonexcited CH_3; thus, as expected, QCT results in CH_3 products with less vibrational energy than ZPVE. Therefore, two sets of results are considered in this section. One of them uses all the trajectories regardless the internal energy of CH_3. Another result, called ZPVE constrained, is based only on trajectories in which the CH_3 products have at least the corresponding ZPVE.

The computed and experimental vibrational and rotational distributions of HF are given in Table XV. The normalized vibrational populations, i.e., $\Sigma_{v,J}\langle P_{v,J}\rangle=1$, are shown in Fig. 6, while the normalized rotational distributions, i.e., $\Sigma_J\langle P_{v,J}\rangle=1$ for each v, corresponding to $v=1-3$ are plotted in Fig. 7. If CH_3 has less internal energy than ZPVE, the most populated HF vibrational state is $v=3$; thus, the $v=3$ vibrational state is overpopulated if the ZPVE constraint is not employed. The use of the ZPVE constraint decreases the $v=3$ vibrational population from 35.0% to 17.5%. The constrained results are in good agreement with experiment since the relative computed (experimental) vibrational populations (all in %) are 0.1(3.8), 14.6(18.9), 67.8(66.7), and 17.5(10.6) corresponding to the $v=0$, 1, 2, and 3 states, respectively. Note that the experimental $v=0$ value ($3.8\pm4.0\%$) has an extremely large error bar, thus it is likely that much less than 1% of the HF products are in the vibrational ground state as the QCT results show. It is important to emphasize that about 2/3 of the HF products correspond to the $v=2$ excited state. Furthermore, both the computed and experimental results show that most of the HF molecules preferentially populate a reduced number of specific rovibrational states (v,J) of all those energetically accessible; since the computed (experi-

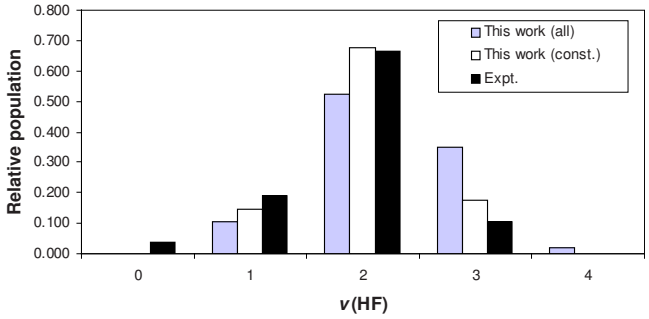

FIG. 6. (Color online) Calculated and experimental normalized HF vibrational populations at collision energy of 630 cm^{-1}. The QCT results denoted as "all" and "const." consider all the trajectories and results without the trajectories that resulted in CH_3 product with internal energy less than its ZPVE, respectively. The experimental (expt.) results were taken from Ref. 11.

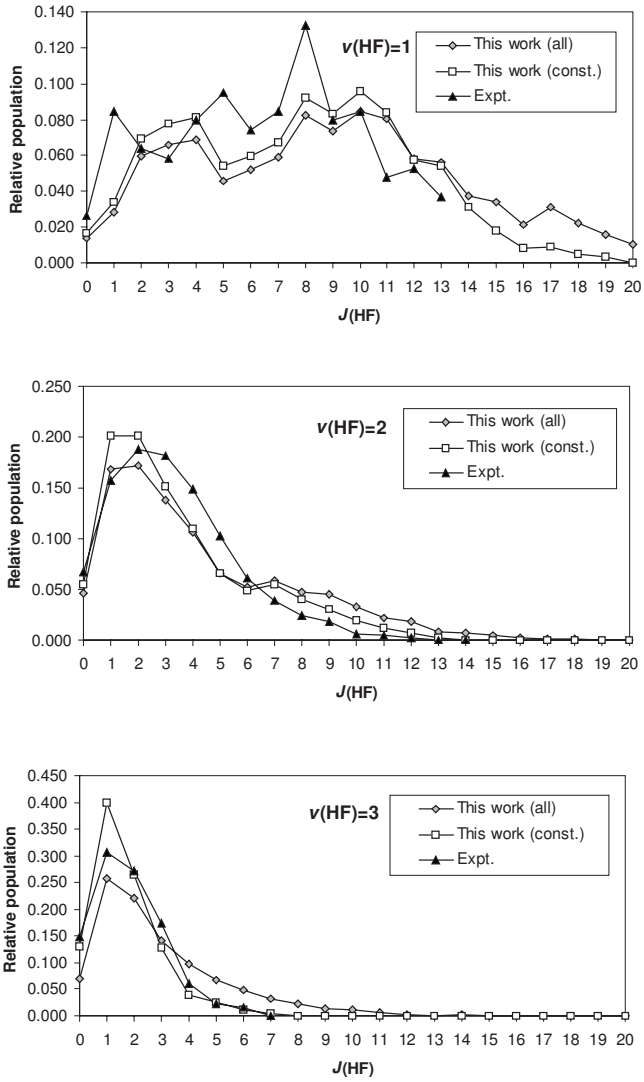

FIG. 7. Calculated and experimental normalized HF rotational populations at collision energy of 630 cm^{-1}. The QCT results denoted as "all" and "const." consider all the trajectories and results without the trajectories that resulted in CH_3 product with internal energy less than its ZPVE, respectively. The experimental (expt.) results were taken from Ref. 11.

mental) populations (in %) of the states (2,1), (2,2), (2,3), and (2,4) are 13.7(10.5), 13.6(12.5), 10.2(12.1), and 7.4(9.9), respectively. Therefore, both theory and experiment agree that nearly half of the HF molecules are produced in these four rovibrational states. The rotational populations plotted in Fig. 7 also agree very well with the experimental results. Both the QCT and experimental results show complicated features at $v=1$ where rotational states with relatively large J values, i.e., $J>10$, also have significant populations. With the increase in the vibrational excitations, the HF molecule tends to be rotationally colder. Both our QCT study and the experiment show that the rotationally most populated states are $J=0-6$ and $J=0-4$ for $v=2$ and 3, respectively. The maximum of the computed (experimental) rotational populations at the vibrational states $v=2$ and 3 are at $J=1\approx2(2)$ and 1(1), respectively. Most of the previous QCT work could not reproduce this feature of the experiment and produced rotationally too hot HF products.

Finally, a note is given regarding the vdW complex in

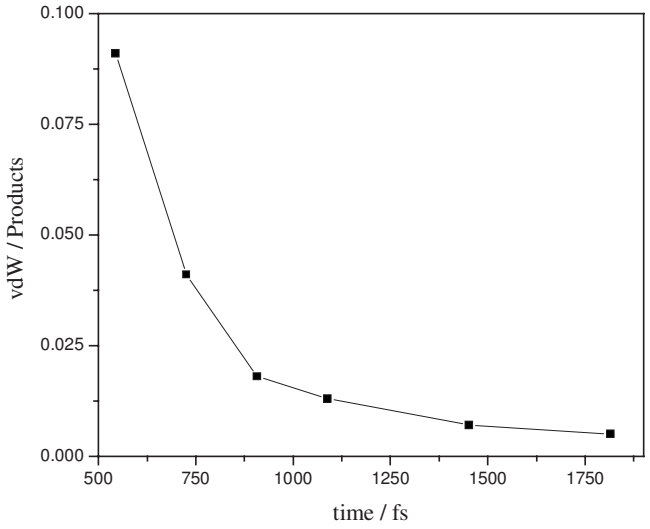

FIG. 8. Branching ratio of the trajectories that resulted in vdW complexes or products as a function of the maximum integration time at collision energy of 630 cm^{-1}.

the product valley. Since this vdWP minimum is below the product asymptote by more than 1000 cm^{-1} and the D_0 value is >400 cm^{-1}, one can assume that some trajectories form a complex whose lifetime can be more than 1 ps. The branching ratio of the nondissociated $(CH_3\text{- - -}HF)_{vdW}$ complexes and the products $(HF+CH_3)$ as a function of the integration time is shown in Fig. 8. The results show that within 545 fs about 10% of the reactive trajectories produce a vdWP complex, while the ratio decreases below 1% beyond about 1200 fs. This is the reason why the maximum integration time of 20 000 time steps (1452 fs) was chosen for the QCT calculations at 630 cm^{-1}. The above-mentioned branching ratio of vdWP and products increases at lower collision energies and, on the other hand, almost all the vdWP complexes dissociate after 726 fs at collision energies higher than 1000 cm^{-1}.

Angular distributions have also been computed at the collision energy of 630 cm^{-1}. The HF vibrationally state-resolved differential cross sections show a vibrational state dependence in the angular distributions. The $HF(v=1,2)$ products are mainly backward scattered with significant contributions in the sideways direction, whereas the $HF(v=3)$ distribution is almost isotropic. A full analysis of this behavior will be presented in a future publication; however, it does appear that the product vdW well is playing a role in those distributions especially for $HF(v=3)$.

B. Excitation function

The excitation function, i.e., cross sections as a function of the collision energy (E_{coll}), of the $F+CH_4\rightarrow HF+CH_3$ reaction has been obtained by performing QCT calculations at 11 different collision energies in the 30–2500 cm^{-1} range. The impact parameter was scanned from 0 to b_{max} with a step size of 1.0 bohr and 500 trajectories were computed at each b. The impact parameter dependence of the reaction probability at different collision energies is shown in Fig. 9. The value of b_{max} increases with the decrease of E_{coll}, e.g. the b_{max} values are 7, 9, 11, and 12 bohr at collision energies

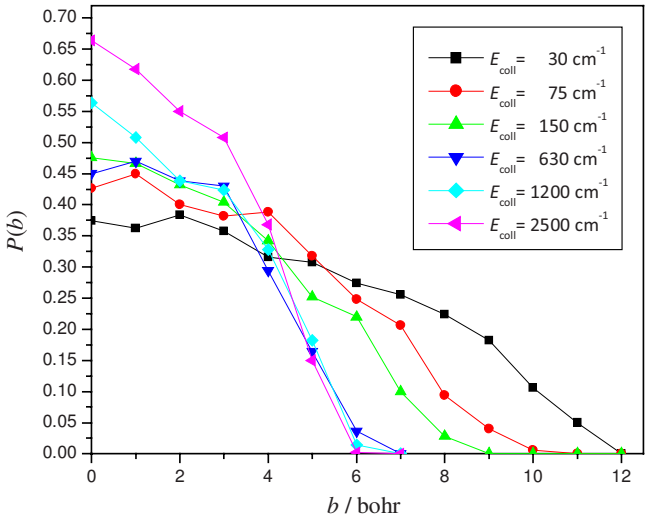

FIG. 9. (Color online) Probability of the F+CH$_4$→HF+CH$_3$ reaction as a function of the impact parameter (b) at different collision energies.

630, 150, 75, and 30 cm^{-1}, respectively. At higher collision energies, i.e., 630–2500 cm^{-1}, b_{max} is around 6–7 bohr and depends just slightly on E_{coll}. The trajectories were integrated up to 30000 (2178 fs) and 10000 (726 fs) time steps in the E_{coll} ranges of 30–450 and 630–2500 cm^{-1}, respectively.

The calculated excitation function is shown in Fig. 10. Considering all the trajectories, the excitation function first decreases rapidly with increasing collision energy and above 450 cm^{-1} becomes nearly flat and independent of the collision energy. The relatively large cross sections and b_{max} values at low collision energies indicate a significant vdW well in the entrance channel. Indeed, our PES contains the stationary points in the vdWR region, however, the D_e values of the C–H$_b$–F(second-order saddle point) and H–C–F (minimum) vdWR complexes are 352 and 363 cm^{-1} on the PES, respectively, whereas the high-level non-SO (SO effect) *ab initio* vales are 42(−3) and 211(−53) cm^{-1}, in order. Therefore, it

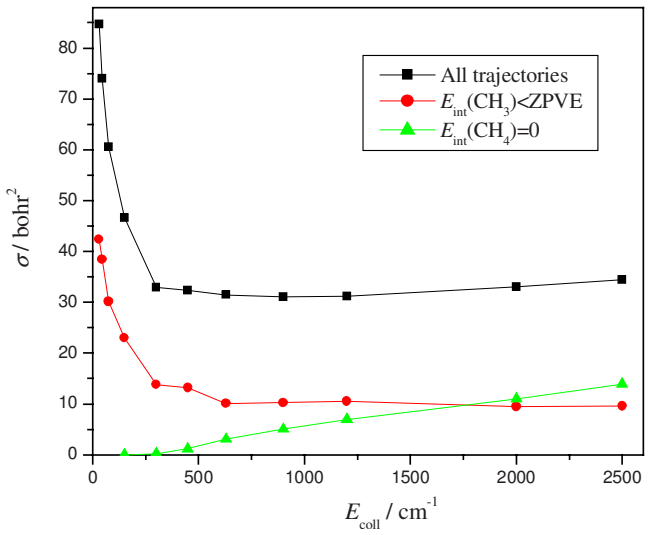

FIG. 10. (Color online) Excitation function of the F+CH$_4$→HF+CH$_3$ reaction. The QCT results consider all the trajectories, trajectories that resulted in CH$_3$ product with internal energy less than its ZPVE, and trajectories initialized without zero-point energy for CH$_4$.

seems that the PES does not describe the entrance channel accurately and this can be a partial reason for the large cross sections at low collision energies. Furthermore, as the *ab initio* results show, the SO effect is significant in this vdWR region of the PES. Work along this direction is in progress.

A threshold energy where the cross section vanishes has not been found. It can be explained by considering the value of the saddle point barrier height of the reaction. The classical barrier height is 167 cm^{-1} corresponding to the PES. However, the ZPVE correction for the barrier height is −181 cm^{-1} based on the harmonic frequencies corresponding to the saddle point and reactant minimum of the PES. Therefore, the ZPVE corrected saddle point barrier height is below zero; thus this is a possible reason why our QCT study, where the initial internal energy of CH$_4$ was set to the ZPVE value, cannot find a threshold collision energy. Furthermore, the PES does not contain a SO correction, which would increase the barrier height by 123 cm^{-1} as discussed in Sec. VI C. We note that experiment found a threshold of <175 cm^{-1} (<0.5 kcal/mol as originally reported).[12] In order to study the effect of the ZPVE, the QCT calculations were also performed initializing the trajectories with zero internal energy for CH$_4$. The cross sections at different collision energies obtained from these trajectories are also shown in Fig. 10. We note that for these calculations the value of x, which is the initial C–F distance at b=0, was increased from 10 to 15 bohr in order to ensure that the initial potential energy does not differ from the asymptotic value of the reactant channel. Unlike the former calculations, this new set of results shows that b_{max} increases with the increase of E_{coll} and the b_{max} values are smaller than the former ones, i.e., b_{max} goes from 3 to 6 bohr in the E_{coll} range of 300–2500 cm^{-1}. Furthermore, the reaction probability decreases drastically in the impact parameter range of 0–1 bohr, especially at low collision energies. The cross sections have a very different E_{coll} dependence, as well. In this case a threshold energy of about 150–300 cm^{-1} has been found and the excitation function values in the E_{coll} range of 300–2500 cm^{-1} are well below the corresponding results obtained with the use of the proper ZPVE for CH$_4$.

Shiu *et al.*[12] measured the state-specific excitation function for CH$_3$(v=0), which rises sharply from the threshold of <175 cm^{-1}, has a peak near 900 cm^{-1}, and decreases rapidly beyond the peak. We did not attempt to do a semiclassical assignment of the CH$_3$ vibrational energy here and so we cannot make a direct comparison with these experiments. We do plan to do that in a future publication. In Fig. 10 we show cross sections obtained from trajectories that resulted in CH$_3$ product with less energy than ZPVE. This excitation function shows a slight decay at increasing collision energies, but obviously does not reproduce the experiment. In Fig. 11 the internal energy distribution of CH$_3$ is shown at collision energies of 150, 630, and 2500 cm^{-1}. All the distributions have a Gauss-type feature and they are blueshifted slightly with the increase in E_{coll}. The expectation values of the internal energies are 6353, 7018, and 7347 cm^{-1} at 150, 630, and 2500 cm^{-1} collision energies, respectively. Note that the ZPVE of CH$_3$ is 6424 cm^{-1}, while the first excited vibrational state is above the ZPVE by only 598 cm^{-1}.

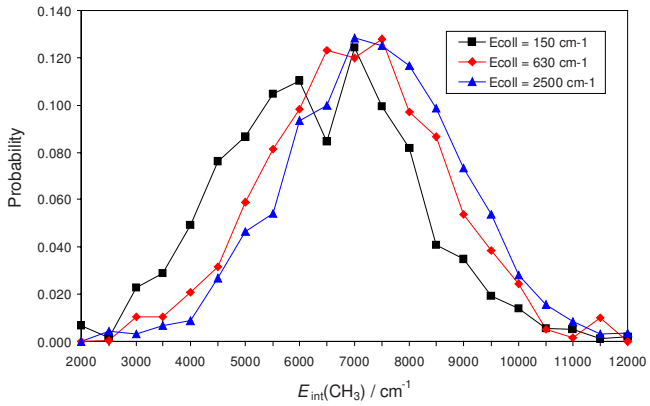

FIG. 11. (Color online) Internal energy distribution of CH_3 at collision energies of 150, 630, and 2500 cm^{-1}.

Therefore, the decay of the state-specific measured excitation function may be explained by the decrease of the fraction of the $CH_3(v=0)$ products at increasing collision energies.

VIII. CONCLUSIONS

A full (12)-dimensional *ab initio* PES of the $F+CH_4 \rightarrow HF+CH_3$ reaction has been developed by fitting 19 384 energy points. This analytical PES is represented by a polynomial expansion in Morse-like variables of the internuclear distances using a basis that is invariant under permutations of like atoms. The energy points for the open-shell (doublet) FCH_4 complex system have been obtained by employing an efficient composite approach, which utilizes UCCSD(T)/aug-cc-pVDZ energies, while the basis set effects are estimated by calculating the differences between UMP2/aug-cc-pVTZ and UMP2/aug-cc-pVDZ energies [see Eq. (1)]. It has been shown that this composite method provides near UCCSD(T)/aug-cc-pVTZ quality energy points, while significantly reducing the computational expenses, and thus represents an attractive approach for the construction of global PESs for dynamical studies.

The PES has a nonlinear first-order saddle point, separating reactants from products, with $C-H_b-F$ angle of about 152° computed at AE-UCCSD(T)/aug-cc-pCVTZ level of theory (see Fig. 2). We note that both the RMP2 and UMP2 methods predict a collinear SP structure. The $C-H_b$ bond length is stretched by 0.023 Å with respect to the bond length in the free CH_4 and the H_b-F distance is 1.621 Å. Since the F^-CH_4 anion complex is being used as a precursor in photodetachment spectroscopy to probe details of the reaction dynamics of the neutral system,[45] it is interesting to note that the H_b-F separation in the anion complex[43] is longer by 0.235 Å than the corresponding distance at the SP of the neutral system. In the reactant valley of the PES, there is a vdW minimum with C_{3v} point-group symmetry and H–C–F linear bond arrangement (see Fig. 2). As high-level *ab initio* computations including spin-orbit effects show the C–F equilibrium distance is 3.045 Å for the above-mentioned vdW complex, while the vdWR minimum is below the dissociation limit by about 160 cm^{-1}. In the product channel a relatively deep vdW minimum can be found; since the D_e and D_0 values of the $(CH_3\text{- - -}HF)_{vdW}$ complex are 1070 and 460 cm^{-1}, respectively. The $C-H_b$ separation in this complex is 2.142 Å, while the C–H and H_b-F equilibrium distances of the complex (corresponding monomer) are 1.078(1.077) and 0.925(0.917) Å, respectively, at the AE-UCCSD(T)/aug-cc-pCVQZ level of theory. As part of the present study variational vibrational calculations have been performed for the $(CH_3\text{- - -}HF)_{vdW}$ complex in full (12) dimension. The *ab initio* UCCSD(T)/aug-cc-pVTZ harmonic frequency for the HF fundamental of the complex is 3940 cm^{-1}, while the variationally computed anharmonic correction is −154 cm^{-1}. Thus our best estimate for this HF stretching fundamental is 3786 cm^{-1} which is in good agreement with the observed vibrational band of 3797 cm^{-1} in helium nanodroplets.[46]

The best technically feasible thermochemical data, such as SP barrier height, dissociation energy of $(CH_3\text{- - -}HF)_{vdW}$, and the reaction enthalpy, have been determined using the composite FPA approach. The barrier height highly depends on the level of the treatment of electron correlation, since the ROHF, RMP2, UCCSD, UCCSD(T), UCCSDT, and UCCSDT(Q) classical BO barrier heights are 3292, 1080, 628, 194, 144, and 109 cm^{-1}, respectively. The computed spin-orbit effect is −8.1 cm^{-1} at the SP, whereas it is −131.5 cm^{-1} for the F atom. Thus the SO correction increases the SP barrier height by +123 cm^{-1}. Our best estimate (including DBOC and scalar relativistic corrections as well) for the vibrationless barrier height is 240 ± 40 cm^{-1}. For the D_e of $(CH_3\text{- - -}HF)_{vdW}$ the CBS limit of the AE-UCCSD(T) results provides a quite accurate value; since the post-UCCSD(T) correlation effects are smaller than 10 cm^{-1} and all the auxiliary corrections, i.e., SO, scalar relativistic, and DBOC, are negligibly small. In the case of the reaction enthalpy the CBS AE-UCCSD(T) result is also accurate enough, due to the fact that the correlation effects beyond the UCCSD(T) level cancel each other. However, the scalar relativistic correction (+61 cm^{-1}) and the SO effect (+132 cm^{-1}) have to be considered in order to achieve the high accuracy. Furthermore, a thermal correction of 202 cm^{-1} has to be employed to convert the enthalpy from 0 to 298.15 K.

The reaction dynamics have been studied by performing QCT calculations, where the required electronic energies and gradients were obtained by numerical differentiation of the new PES. The computed (measured[11]) HF vibrational populations (in %) at collision energy of 630 cm^{-1} are 0.1(3.8), 14.6(18.9), 67.8(66.7), and 17.5(10.6) corresponding to the $v=0$, 1, 2, and 3 states, respectively. Thus, both theory and experiment have found within excellent qualitative agreement that about 2/3 of the HF products are in the vibrationally excited $v=2$ state. Unlike most of the previous QCT studies, our trajectories do not produce rotationally too hot HF products. The experimentally observed maxima of the rotational populations are at $J=2$ and 1 for the vibrational states $v=2$ and 3, respectively, and our QCT results show the same feature. Cross sections have also been determined at different collision energies in the range of 30–2500 cm^{-1}. The cross sections increase with the decrease in the collision energy, and we have not found a threshold energy. However, if trajectories are initiated with zero internal energy in the CH_4 reactant then a threshold collision energy between 150

and 300 cm^{-1} is observed. The internal energy of the CH_3 product slightly increases with the collision energy; since the expectation values of the internal energies are 6353, 7018, and 7347 cm^{-1} at collision energies of 150, 630, and 2500 cm^{-1}, respectively. This predicts that CH_3 is at the vibrational ground state (ZPVE is 6424 cm^{-1}) at low collision energies, however, significant fraction of the CH_3 products can be vibrationally excited at higher collision energies due to the fact that the umbrella-bending fundamental of CH_3 is only 598 cm^{-1}.

Finally, we note the similarities of the F+CH_4 and the prototypical F+H_2 (see Ref. 49 for further details) reactions: (a) both reactions are exothermic having almost the same reaction enthalpy; (b) the product HF molecules are vibrationally excited; (c) the high level of electronic structure theory gives noncollinear saddle point structures with low barrier heights; (d) the spin-orbit coupling increases the barrier heights by about 120 cm^{-1} in both cases; (e) vdW minima exist in the entrance valley and $(CH_4\text{- - -F})_{vdW}$ does not have C–H–F bond arrangement, but H–C–F, while $(H_2\text{- - -F})_{vdW}$ is not linear, but T-shaped; and (f) in the exit channel the complexes $(CH_3\text{- - -HF})_{vdW}$ and $(H\text{- - -HF})_{vdW}$ have collinear equilibrium structures.

ACKNOWLEDGMENTS

Discussions with Mr. E. Garand and Professor D. M. Neumark on F–CH_4 are gratefully acknowledged. G. C. thanks Professor A. G. Császár for his help with the MRCC computations. Discussions with Dr. A. C. Simmonett on the open-shell CC methods are also acknowledged. We acknowledge that this work is partially conducted under the auspices of the iOpenShell Center for Computational Studies of Electronic Structure and Spectroscopy of Open-Shell and Electronically Excited Species supported by the National Science Foundation through CRIF:CRF Grant No. CHE-0625419 +0624602+0625237. Financial support from the Office of Naval Research (Grant No. N00014-05-1-0460) and the Department of Energy (Grant No. DE-FG02-97ER14782) is also acknowledged.

[1] D. E. Manolopoulos, J. Chem. Soc., Faraday Trans. **93**, 673 (1997).
[2] A. Gauss, Jr., J. Chem. Phys. **65**, 4365 (1976).
[3] J. C. Corchado and J. Espinosa-García, J. Chem. Phys. **105**, 3160 (1996).
[4] H. Kornweitz, A. Persky, and R. D. Levine, Chem. Phys. Lett. **289**, 125 (1998).
[5] C. Rángel, M. Navarrete, and J. Espinosa-García, J. Phys. Chem. A **109**, 1441 (2005).
[6] D. Troya, J. Millan, I. Banos, and M. Gonzalez, J. Chem. Phys. **120**, 5181 (2004).
[7] J. F. Castillo, F. J. Aoiz, L. Banares, E. Martinez-Nunez, A. Fernandez-Ramos, and S. Vazquez, J. Phys. Chem. A **109**, 8459 (2005).
[8] D. Troya, J. Chem. Phys. **123**, 214305 (2005).
[9] O. Roberto-Neto, F. B. C. Machado, and F. R. Ornellas, Chem. Phys. **315**, 27 (2005).
[10] J. Espinosa-García, J. L. Bravo, and C. Rangel, J. Phys. Chem. A **111**, 2761 (2007).
[11] W. W. Harper, S. A. Nizkorodov, and D. J. Nesbitt, J. Chem. Phys. **113**, 3670 (2000).
[12] W. Shiu, J. J. Lin, K. Liu, M. Wu, and D. H. Parker, J. Chem. Phys. **120**, 117 (2004).
[13] W. Shiu, J. J. Lin, and K. Liu, Phys. Rev. Lett. **92**, 103201 (2004).
[14] Q. Wang, Z. Cai, and D. Feng, J. Mol. Struct.: THEOCHEM **759**, 31 (2006).
[15] W. D. Allen, A. L. L. East, and A. G. Császár, in *Structures and Conformations of Non-Rigid Molecules*, edited by J. Laane, M. Dakkouri, B. van der Veken, and H. Oberhammer (Kluwer, Dordrecht, 1993), p. 343.
[16] A. G. Császár, W. D. Allen, and H. F. Schaefer, J. Chem. Phys. **108**, 9751 (1998).
[17] G. Czakó, E. Mátyus, A. C. Simmonett, A. G. Császár, H. F. Schaefer, and W. D. Allen, J. Chem. Theory Comput. **4**, 1220 (2008).
[18] M. S. Gordon and D. G. Truhlar, J. Am. Chem. Soc. **108**, 5412 (1986).
[19] T. H. Dunning, Jr., J. Chem. Phys. **90**, 1007 (1989).
[20] R. A. Kendall, T. H. Dunning, Jr., and R. J. Harrison, J. Chem. Phys. **96**, 6796 (1992).
[21] D. E. Woon and T. H. Dunning, Jr., J. Chem. Phys. **103**, 4572 (1995).
[22] W. J. Hehre, L. Radom, P. v. R. Schleyer, and J. A. Pople, *Molecular Orbital Theory* (Wiley, New York, 1986).
[23] C. Møller and M. S. Plesset, Phys. Rev. **46**, 618 (1934).
[24] J. Čížek, J. Chem. Phys. **45**, 4256 (1966).
[25] K. Raghavachari, G. W. Trucks, J. A. Pople, and M. Head-Gordon, Chem. Phys. Lett. **157**, 479 (1989).
[26] J. D. Watts, J. Gauss, and R. J. Bartlett, J. Chem. Phys. **98**, 8718 (1993).
[27] M. Kállay and J. Gauss, J. Chem. Phys. **123**, 214105 (2005).
[28] H.-J. Werner, P. J. Knowles, R. Lindh *et al.*, MOLPRO, Version 2006.1, a package of *ab initio* programs (see http://www.molpro.net).
[29] M. Kállay, MRCC, a string-based quantum chemical program suite (for the latest version, see http://mrcc.hu).
[30] M. Kállay and P. R. Surján, J. Chem. Phys. **115**, 2945 (2001).
[31] J. F. Stanton, J. Gauss, J. D. Watts, P. G. Szalay, and R. J. Bartlett with contributions from A. A. Auer, D. B. Bernholdt, O. Christiansen, M. E. Harding, M. Heckert, O. Heun, C. Huber, D. Jonsson, J. Jusélius, W. J. Lauderdale, T. Metzroth, C. Michauk, D. P. O'Neill, D. R. Price, K. Ruud, F. Schiffmann, M. E. Varner, and J. Vázquez, the Mainz–Austin–Budapest version of ACES II and the integral packages MOLECULE (J. Almlöf and P. R. Taylor), PROPS (P. R. Taylor), and ABACUS (T. Helgaker, H. J. Aa. Jensen, P. Jørgensen, and J. Olsen).
[32] N. C. Handy, Y. Yamaguchi, and H. F. Schaefer, J. Chem. Phys. **84**, 4481 (1986).
[33] T. D. Crawford, C. D. Sherrill, E. F. Valeev, J. T. Fermann, R. A. King, M. L. Leininger, S. T. Brown, C. L. Janssen, E. T. Seidl, J. P. Kenny, and W. D. Allen, J. Comput. Chem. **28**, 1610 (2007).
[34] M. Douglas and N. M. Kroll, Ann. Phys. **82**, 89 (1974).
[35] A. Berning, M. Schweizer, H.-J. Werner, P. J. Knowles, and P. Palmieri, Mol. Phys. **98**, 1823 (2000).
[36] M. J. Frisch, G. W. Trucks, H. B. Schlegel *et al.*, GAUSSIAN 03, Revision C.02, Gaussian, Inc., Wallingford, CT, 2004.
[37] S. Carter, J. M. Bowman, and N. C. Handy, Theor. Chem. Acc. **100**, 191 (1998).
[38] J. M. Bowman, S. Carter, and X. Huang, Int. Rev. Phys. Chem. **22**, 533 (2003).
[39] J. K. G. Watson, Mol. Phys. **15**, 479 (1968).
[40] J. O. Jung and R. B. Gerber, J. Chem. Phys. **105**, 10332 (1996).
[41] S. Carter, S. J. Culik, and J. M. Bowman, J. Chem. Phys. **107**, 10458 (1997).
[42] J. Wu, X. Huang, S. Carter, and J. M. Bowman, Chem. Phys. Lett. **426**, 285 (2006).
[43] G. Czakó, B. J. Braams, and J. M. Bowman, J. Phys. Chem. A **112**, 7466 (2008).
[44] Z. Xie, J. M. Bowman, and X. Zhang, J. Chem. Phys. **125**, 133120 (2006).
[45] D. M. Neumark, personal communication (Nov. 2, 2007).
[46] J. M. Merritt, S. Rudić, and R. E. Miller, J. Chem. Phys. **124**, 084301 (2006).
[47] A. Karton and J. M. L. Martin, Theor. Chem. Acc. **115**, 330 (2006); W. Klopper and W. Kutzelnigg, J. Mol. Struct.: THEOCHEM **135**, 339 (1986); G. Tasi and A. G. Császár, Chem. Phys. Lett. **438**, 139 (2007).
[48] T. Helgaker, W. Klopper, H. Koch, and J. Noga, J. Chem. Phys. **106**, 9639 (1997).
[49] K. Stark and H.-J. Werner, J. Chem. Phys. **104**, 6515 (1996).
[50] D. L. Gray and A. G. Robiette, Mol. Phys. **37**, 1901 (1979).
[51] D. M. Medvedev, L. B. Harding, and S. K. Gray, Mol. Phys. **104**, 73 (2006).
[52] E. A. Shenyavskaya and V. S. Yungman, J. Phys. Chem. Ref. Data **33**, 923 (2004).